THE OPTIMIZED SCHWARZ METHOD WITH A COARSE GRID CORRECTION[*]

OLIVIER DUBOIS[†], MARTIN J. GANDER[‡], SÉBASTIEN LOISEL[§], AMIK ST-CYR[¶], AND DANIEL B. SZYLD[‖]

Abstract. Optimized Schwarz Methods (OSM) use Robin transmission conditions across the subdomain interfaces. The Robin parameter can then be optimized to obtain the fastest convergence. A new formulation is presented with a coarse grid correction. The optimal parameter is computed for a model problem on a cylinder, together with the corresponding convergence factor which is smaller than that of classical Schwarz methods. A new coarse space is presented, suitable for OSM. Numerical experiments illustrating the effectiveness of OSM with a coarse grid correction, both as an iteration and as a preconditioner, are reported.

1. Introduction. A popular and quite effective method for solving large elliptic problems is to subdivide the domain into many subdomains, and solve smaller elliptic problems on each subdomain in parallel. The Schwarz iteration reconciles these local solutions by using Dirichlet boundary conditions on the artificial interfaces between the subdomains and iterating; see, e.g., [40], [45]. These methods are also used as preconditioners. The idea of Optimized Schwarz Methods (OSM) is to use different boundary conditions on the artificial interfaces, such as Robin conditions, and take advantage of the fact that the Robin parameter can be optimized to obtain a faster convergence; see below for references.

It is well-known that a coarse grid correction improves the convergence of the classical Schwarz methods, and in fact it is necessary in order to obtain *weak scaling*. An algorithm scales weakly if it can solve a larger problem in reasonable time by increasing the number of processors.[1]

In this article, we introduce an optimized Schwarz method with a coarse grid correction, which we call Coarse-grid Optimized of Order 0 (CO0 for short). This is the first time that a coarse grid correction for OSM is analyzed. In fact, this is the first time that an optimized parameter is calculated for an OSM with multiple subdomains. We consider a version of the method with overlap (Section 3) and one without overlap (Section 4). We analyze these new formulations on a model problem, namely the Laplacian on a cylinder, described in detail in Section 2. For this model problem, we are able to study in detail the convergence properties of the method for any number of subdomains, including the computation of an optimal parameter, and the corresponding convergence factor. We show that for our model problem CO0 has better weak scaling properties than the classical alternating Schwarz method with a coarse grid correction (Section 5). We describe implementation details for general domains of the CO0 algorithm using a Restricted Additive Schwarz iteration, and we introduce a proposed coarse space (Section 6). In Sections 7 and 8 we present numerical experiments illustrating the convergence of the new CO0 methods. We end with some conclusions in Section 9, which is followed by an Appendix which contains some of the more technical proofs.

We now outline the history of Optimized Schwarz Methods, and refer to [15] and [16] for further details, as well as a complete derivation for Helmholtz and Laplace problems in the plane. The optimized Schwarz method was introduced in [6], [36], [37], under various names. The OSM has one or more free parameters which need to be chosen carefully to obtain the best possible convergence. Several efforts were undertaken to find, for different differential equations and/or suitable domains, the best possible parameter choices; see, e.g., [20], [22], [23], [24], [25].

The usual approach for optimizing the free parameters is to take a Fourier transform of the partial differential equation, obtaining an explicit recurrence relation for the iteration. This works only in special

[1]The usual statement is that an algorithm scales weakly if it can solve a problem that is twice the size using twice the number of processors in the same amount of time. The classical Schwarz method with a coarse grid correction can be shown to scale weakly in this sense, as long as we neglect the cost of communication and the cost of calculating the coarse grid correction. See Section 5 for further details.

cases, for example, if the domain is a rectangle and the differential operator is the Laplacian with homogeneous Dirichlet conditions. In addition to the Laplace and Helmholtz problems, the method can be used for various other canonical problems; see [3], [12], [18], [19], [31], [33] for convection-diffusion problems, [17], [21] for the wave equation, [1], [9] for Maxwell's equations, [10] for fluid dynamics, and [34], [39] for the shallow water equation. As already mentioned, in these references, and others, one could only consider relatively simple domains. Proofs of convergence for more general situations have been recently obtained [26], [29]; but the techniques used are not amenable to finding the optimal parameters. A proof of convergence for the nonoverlapping algorithm was provided in [27], using energy estimates; see also [30]. We mention in passing that one way of obtaining convergence of the nonoverlapping algorithm, is to define a relaxation of the method [8].

In the analysis of our CO0 method, we take an approach similar to that in the rest of the literature in this field, and consider a model problem. We choose the Laplacian on a cylinder, where the subdomains are overlapping vertical strips. By making this choice, we can analyze the methods by taking a Fourier transform in the vertical direction and estimating the eigenvalues of the iteration matrix. As we shall see, this allows us to bound the convergence of the method with the coarse grid correction as well as to compute the optimal Robin parameter. Numerical experiments for this model problem illustrate the theoretical results. Experiments with other configurations, including meshes with cross-points are also presented, in which the form of the optimal parameters computed for the model problems are shown to be useful as well in more general situations. The experiments also show that the coarse grids developed in the paper work well.

The major innovation of our paper is the addition of a coarse grid to optimized Schwarz methods. This is essential for such methods to make them scalable, and our paper contains to the best of our knowledge the first convergence analysis of an optimized Schwarz method with a coarse grid correction.

The analysis of optimized Schwarz methods is much harder than the analysis of classical Schwarz methods, because the iterates are discontinuous, and thus none of the abstract Schwarz theory developed for the additive Schwarz method can be used. We develop rigorous convergence estimates for a very specially chosen model decomposition. The tools used in this analysis unfortunately do not carry over to more general decompositions. While the analysis is only valid for our model decomposition, we test numerically the optimized Schwarz method with coarse grid correction for the fully general case, including cross points, for various finite difference, finite element and spectral element discretizations in Sections 7 and 8. In each case, the method performs as predicted by our analysis for the model situation.

We denote by A^* the conjugate-transpose of matrix A, and by $\Re z$ and $\Im z$ the real and imaginary parts of $z \in \mathbb{C}$, respectively. As usual, $O(g)$ stands for a function whose magnitude is bounded above by a constant times g while $\Omega(g)$ stands for a function whose magnitude is bounded below by a constant times g. In Section 5, we neglect polylogarithmic terms, hence $O(g)$ stands for a function whose magnitude is bounded by a polylogarithm times g.

2. The model problem and the CO0 method. The model problem we consider is to solve the Laplacian on a cylinder, i.e., on the domain $\Omega = (\mathbb{R}/JH\mathbb{R}) \times (0, a)$ with periodic boundary conditions at $x = 0$ and JH, and with homogeneous Dirichlet data at $y = 0$ and a. Thus, the goal is to solve the elliptic boundary value problem

$$\begin{cases} \Delta u = f & \text{in } \Omega, \\ u(x,0) = u(x,a) = 0 & \text{for all } x \in \mathbb{R}/JH\mathbb{R}, \\ u(0,y) = u(JH,y) & \text{for all } y \in (0,a), \\ u_x(0,y) = u_x(JH,y) & \text{for all } y \in (0,a). \end{cases} \tag{2.1}$$

with data f and unknown u. We emphasize now that we are looking for solutions which are periodic in x, which is why we use the notation $x \in \mathbb{R}/JH\mathbb{R}$ in (2.1).

We consider J overlapping subdomains consisting of vertical strips given by

$$\Omega_j = \left(\left(j - \frac{1}{2} \right) H - \frac{L}{2}, \left(j + \frac{1}{2} \right) H + \frac{L}{2} \right) \times (0,a), \quad j \in \mathbb{Z}/J\mathbb{Z}.$$

Therefore, there are J subdomains, and the overlap is of width L. We have again emphasized the periodicity in x, by using $j \in \mathbb{Z}/J\mathbb{Z}$. In particular, we have that $\Omega_0 = \Omega_J$, and we can speak of the neighbors Ω_{j+1} and Ω_{j-1} to the subdomain Ω_j, for each $j = 1, \ldots, J$.

An equivalent formulation of the model problem (2.1) taking into account the overlapping subdomains and imposing Robin boundary conditions on the artificial interfaces is the following augmented system:

$$\begin{cases} \Delta v_j &=& f \text{ in } \Omega_j, \\ v_j(x,0) &=& v_j(x,a) = 0 \text{ for all } x \in \mathbb{R}/JH\mathbb{R}, \\ (p+D_x)v_j|_{x=(j+1/2)H+L/2} &=& (p+D_x)(v_{j+1})|_{x=(j+1/2)H+L/2}, \\ (p-D_x)v_j|_{x=(j-1/2)H-L/2} &=& (p-D_x)(v_{j-1})|_{x=(j-1/2)H-L/2}; \end{cases} \quad (2.2)$$

for $j = 1, \ldots, J$, where the coefficient $p > 0$ is a Robin parameter, which we may choose in any way we prefer, provided the subdomain problems are well posed, and where v_{J+1} is understood to be v_1.

LEMMA 2.1. *The system (2.2) has a unique solution $\{v_j\}$. This unique solution has the property that $v_j = v_{j+1}$ on $\Omega_j \cap \Omega_{j+1}$, $j = 1, \ldots, J$. By gluing the local solutions v_j together, we obtain $v \in H_0^1(\Omega)$ with $v = u$ is the unique solution of (2.1).*

Proof. Assume that we have a solution $\{v_j\}$ of (2.2). Let $j \in \{1, \ldots, J\}$ and consider the "overlap problem"

$$\begin{cases} \Delta w &=& f \text{ in } \Omega_j \cap \Omega_{j+1}, \\ w(x,0) &=& w(x,a) = 0 \text{ for all } x \in \mathbb{R}/JH\mathbb{R}, \\ (p+D_x)w|_{x=(j+1/2)H+L/2} &=& (p+D_x)(v_{j+1})|_{x=(j+1/2)H+L/2}, \\ (p-D_x)w|_{x=(j+1/2)H-L/2} &=& (p-D_x)(v_j)|_{x=(j+1/2)H-L/2}; \end{cases} \quad (2.3)$$

where w is the unknown. Observe that (2.3) has a unique solution w.[2] Furthermore, we note from (2.2) that both $w = v_j$ and $w = v_{j+1}$ solve (2.3). Because the solution of (2.3) is unique, we conclude that $v_j = v_{j+1}$ on $\Omega_j \cap \Omega_{j+1}$. Therefore, we may glue together the solutions $\{v_j\}$ obtaining $v = u$, the unique solution $u \in H_0^1(\Omega)$ to (2.1).

Conversely, if u is the unique solution to (2.1) then setting $v_j = u|_{\Omega_j}$ for every j yields a solution to (2.2). □

A one-level optimized Schwarz iteration with Robin conditions (OO0) is obtained from (2.2) by iteratively enforcing the interface conditions. In order to introduce the coarse grid correction, our starting point is the augmented system (2.2). The "coarse space" is defined as a suitable subspace of $H_0^1(\Omega)$ of small dimension. The coarse grid correction z is defined as the solution to some approximate Laplacian on the coarse space, and it is incorporated in the Robin conditions across the artificial interfaces. Given initial approximations v_j^0 to the solution of (2.2), $j = 1, \ldots, J$, and an initial approximation to the coarse grid correction z^0 (which can be chosen as $z^0 = 0$), the iterative CO0 method can be described as follows:

$$\begin{cases} \Delta v_j^n &=& f \text{ in } \Omega_j, \\ v_j^n(x,0) &=& v_j^n(x,a) = 0 \text{ for all } x \in \mathbb{R}/JH\mathbb{R}, \\ (p+D_x)v_j^n|_{x=(j+1/2)H+L/2} &=& (p+D_x)(v_{j+1}^{n-1} - z^{n-1})|_{x=(j+1/2)H+L/2}, \\ (p-D_x)v_j^n|_{x=(j-1/2)H-L/2} &=& (p-D_x)(v_{j-1}^{n-1} - z^{n-1})|_{x=(j-1/2)H-L/2}; \end{cases} \quad (2.4)$$

for $j \in \mathbb{Z}/J\mathbb{Z}$ and $n = 1, 2, \ldots$, and with the coarse grid correction

$$\begin{cases} \Delta_H z^n &=& (\Delta v^n - f)_H \text{ in } \Omega, \\ z^n &=& 0 \text{ on } \partial\Omega. \end{cases} \quad (2.5)$$

Here, we have used the notation Δ_H for some approximate Laplacian, and the notation $(\cdot)_H$ for some suitable projection of a function to the coarse space. The function v^n must be constructed by gluing the local solutions $v_1^n, \ldots, v_J^n$ in some suitable way. The scalar $p \in \mathbb{R}$ will be chosen in such a way that the method has fast convergence.

When two subdomains Ω_j and Ω_ℓ intersect, then there are multiple function values (one for v_j^n and one for v_ℓ^n) that must be stored on $\Omega_j \cap \Omega_\ell$ (this explains the terminology augmented system). In a computer program, one can implement an iteration using the augmented system, but there is a remarkable correspondence between the iteration on the augmented system and the Restricted Additive Schwarz (RAS) iterations [42],

---

[2]This follows either from the variational theory or, since the overlap is a rectangle, from Fourier sine series.

and thus the RAS approach is a good alternative to gluing the functions v_j^n. This is further discussed in Section 6.[3]

In the next section, we analyze the CO0 method (2.4)–(2.5), proving its geometric convergence with convergence factor $\rho = 1 - C\epsilon^{1/3}$, where C is a constant, and $\epsilon = L/H$ is the ratio between the overlap and the coarse grid parameter. Later, in Section 4, we consider a nonoverlapping version of the CO0 method and we show convergence with a convergence factor $\rho = 1 - C\epsilon^{1/2}$ (for some other constant C), where the small parameter is $\epsilon = h/H$ in that case. By comparison, a classical Schwarz algorithm with a coarse grid correction, when used as a preconditioner, has a condition number $\kappa \leq C(1 + \frac{H}{L})$; see for example [45, section 3.6]. For an iterative Schwarz method with Dirichlet interface conditions and coarse grid correction, although there are no results regarding the convergence factor, we expect (and observe in numerical experiments) the asymptotic behavior $\rho = 1 - C(L/H)$.

3. Convergence of the overlapping CO0 algorithm. For a function $v(x, y)$ on Ω_j or Ω, define the Fourier transform $\hat{v}(x, k)$ by

$$\hat{v}(x, k) = \frac{1}{\sqrt{a}} \int_0^a v(x, y) \sin(ky) \, dy.$$

This choice of the definition of the Fourier transform ensures the simple formula $\widehat{(v_{yy})}(x, k) = -k^2 \hat{v}(x, k)$, independently of a. The frequency variable k takes values in the discrete domain $(\pi/a)\mathbb{N} \subset (0, \infty)$. A function of the form

$$\sum_{k \in (\pi/a)\mathbb{N}, \, k \leq d} \alpha_k \sin ky$$

is called a sine polynomial of degree d.

Let u be the solution of the boundary value problem (2.1). Then, the error iterates $v_j^n - u$ also satisfy the equation (2.4), but with $f = 0$. Therefore, to analyze the convergence of the CO0 method and compute its convergence factor, the simplifying assumption that $f = 0$ is made.

Since $\Delta v_j^n = 0$ in each subdomain, we can "solve" the iteration (2.4) by taking a Fourier transform in y. Indeed, for $n = 1, 2, \ldots$, and for $j \in \mathbb{Z}/J\mathbb{Z}$, we obtain

$$\hat{v}_j^n(x, k) = \alpha_j^n(k)e^{k(x-jH)} + \beta_j^n(k)e^{-k(x-jH)}. \tag{3.1}$$

This particular choice of basis and translation will result in an iteration matrix which is easier to analyze. Indeed, the subdomains are all similar to each other.

For our analysis of the CO0 method (2.4)–(2.5) we use a coarse grid which is "semispectral", with J nodes along the x axis, and with $a/H - 1$ frequencies (we assume that a/H is an integer) along the y axis (the $y = 0$ and $y = a$ points being taken care of by the Dirichlet conditions). The nodes along the x axis are located at $x_j = jH$, $j \in \mathbb{Z}/J\mathbb{Z}$, and consequently each subdomain contains one coarse grid point in the x direction, and there is a total of J coarse grid points in the x direction.

We exploit the geometric structure of our particular domain decomposition and choose the basis functions of the coarse space to be piecewise linear in x, and sine polynomials in y. The basis functions are of the form $\ell(x) \sin ky$, where $\ell(x)$ is a piecewise linear function of x with nodes at $x = 0, H, \ldots, (J-1)H$ and $k \in \{\pi/a, 2\pi/a, \ldots, (a-H)\pi/aH\}$.

Since the coarse grid correction is a sine polynomial in y, it is more natural to express it by giving the Fourier coefficients. Since there are $a/H - 1$ points in the y directions, there should be $a/H - 1$ frequencies in the y direction. Since the grid is semispectral[4], we analyze it separately for the frequencies $k \geq \pi/H$ and $k < \pi/H$. We note that the coarse space is designed to reduce the error in the low frequencies. Therefore, the first requirement for the coarse grid correction is that $\hat{z}^n(x, k) = 0$ for all $k \geq \pi/H$ and all x. This means that, for every x, $z^n(x, y)$ is a sine polynomial in y of degree less than π/H. For frequencies $k < \pi/H$, in the x direction, we assume that for each (discrete) frequency k, the function $\hat{z}^n(x, k)$ is piecewise linear

---

[3]There are also relationships with the Multiplicative Schwarz and Restricted Multiplicative Schwarz iterations, as well as weighted variants.

[4]Spectral methods truncate the information beyond a certain frequency

with vertices at the grid points ℓH, $\ell = 1, 2, \ldots, J$. At each grid point ℓH, and each frequency $k < \pi/H$, $k \in (\pi/a)\mathbb{N}$, we define

$$\hat{z}^n(\ell H, k) = \hat{v}_\ell^n(\ell H, k). \tag{3.2}$$

That is, this particular coarse grid correction computes the exact solution $\hat{u}$ (the Fourier transform of the exact solution u) at the vertices of the coarse grid, for frequencies $k < \pi/H$. Equation (3.2) formally defines the approximation used for the Laplacian in the coarse space.

We are now ready to state our main result.

THEOREM 3.1. *Consider the solution of (2.1) using the CO0 method defined by (2.4) with a coarse grid correction defined as in (3.2). Let $L > 0$ be the thickness of the overlap, and let $H > L$ be the coarse grid parameter, with each subdomain having a width of $(H + L)$, counting the overlap. Let $J \in \mathbb{N}$ be the number of subdomains. When L/H is small, for any $c > 0$, the choice of parameter*

$$p_c^* = cH^{-2/3}L^{-1/3} \tag{3.3}$$

leads to a convergence factor

$$\rho(L, H) = 1 - \min\{2/c, \sqrt{8c}\}(L/H)^{1/3} + O((L/H)^{2/3}). \tag{3.4}$$

Furthermore, if the number of subdomains J is either even or large, and for sufficiently large a, the algorithm diverges if

$$p < \frac{2}{2H - L}. \tag{3.5}$$

The proof of this theorem is rather technical, and it is developed over the next three subsections. Because we also want to show divergence when the parameter p is too small, we must ensure that our estimates are sharp. For that reason, in the proof Lemma 3.7 and elsewhere, we will keep track of the sharpness of our estimates.

In the rest of this subsection, we make several remarks on this result.

REMARK 3.2. *We emphasize that the upper bound (3.4) for the convergence factor estimate depends only on $\epsilon = L/H$, and not on the separate values L and H. This is important, because a standard method to increase the parallelism of the solver is to increase the number of subdomains, as the fine grid parameter h becomes finer. In this situation, if the overlap L is exactly h, and if we keep h/H constant by increasing the number J of subdomains, then the convergence factor estimate (3.4) will not deteriorate as h tends to zero. This is called "weak scaling". Another good scaling property of our estimate is that it does not directly depend on the number J of subdomains, the height a of the cylinder, or the circumference JH of the cylinder (except indirectly inasmuch these variables may be related to L and H in a particular problem).*

REMARK 3.3. *If p is too small, then Theorem 3.1 indicates that the algorithm diverges. In order to guarantee $p_c^* > \frac{2}{2H-L}$ regardless of the values of L, H, ϵ, p, a, one should choose $c > 2$.*

REMARK 3.4. *The important statement in Theorem 3.1 is that the optimized parameter for small ϵ is $p_c^* = O(\epsilon^{2/3}L^{-1})$. Equation (3.4) suggests that $c = 2^{-1/3} \approx 0.7937$ is the best possible, but this is only true when ϵ is very small, and for the specific implementation of the Laplace solver on the cylinder analyzed here, where the subdomains are overlapping strips. In practice, when solving on a general domain with general subdomains, any coefficient c will lead to a convergence factor of $1 - O(\epsilon^{1/3})$. The best possible c can be determined numerically.*

REMARK 3.5. *Although the spectrum $(\pi/a)\mathbb{N}$ is discrete, we will often replace it with a continuum such as $(0, \infty)$ for estimating convergence. This modification has previously been studied in detail in [28] for the spherical Laplacian, which complicates the analysis significantly. It was found that using a continuous spectrum instead of a discrete spectrum did not affect the asymptotic behavior of the methods.*

REMARK 3.6. *In [15], an analysis of the OSM for two subdomains is performed under the assumption that the overlap L is equal to h, the fine grid parameter. In that paper, the optimized parameter $p = p^*$ is given as a function of h and $k_{\min}$, the lowest frequency in the vertical direction. The formula obtained is $p^* = 2^{-1/3}k_{\min}^{2/3}h^{-1/3}$. There is a relationship between p^* and p_c^*. In our case, the lowest frequency*

represented on the domain is $k_{\min} = \pi/a$. *However, the lowest frequency which is not coarse grid corrected is* $k_{cgc} = \pi/H \gg k_{\min}$. *If we set* $k_{\min} = k_{cgc} = \pi/H$ *in the formula for* p^*, *we obtain our parameter* p_c^* *with the constant* $c = (2\pi)^{2/3}/2 \approx 1.7$. *Thus, our analysis seems to validate the heuristic of analyzing a two-subdomain model problem and using the resulting parameter estimate with* J *subdomains and a coarse grid correction, by assuming that the OSM must be optimized for the high frequencies that are not coarse grid corrected; i.e., by using* k_{cgc} *as the lowest resolvable frequency in the two-domain analysis, instead of the usual* $k_{\min}$.

However, this two-subdomain heuristic does not reveal the divergence behavior. The divergence behavior is only revealed by our analysis of the interplay between the coarse grid correction and the Optimized Schwarz Method in the low frequencies.

3.1. The eigenvalues of a block-circulant matrix. We begin with an auxiliary result which gives a formula for the eigenvalue of a block circulant matrix. In short, we will see that our iteration can be rephrased as a power iteration for a 2×2 block matrix T, whose blocks are all "tridiagonal" complex circulant matrices.

LEMMA 3.7. *Let A and B be $J \times J$ "tridiagonal" complex circulant matrices, i.e., of the form*

$$
A = \begin{bmatrix}
a_0 & a_1 & 0 & \ldots & 0 & a_{-1} \\
a_{-1} & a_0 & a_1 & 0 & \ldots & 0 \\
0 & \ddots & \ddots & \ddots & & \vdots \\
\vdots & & \ddots & \ddots & \ddots & 0 \\
0 & & & \ddots & \ddots & a_1 \\
a_1 & 0 & \ldots & 0 & a_{-1} & a_0
\end{bmatrix}, \quad
B = \begin{bmatrix}
b_0 & b_1 & 0 & \ldots & 0 & b_{-1} \\
b_{-1} & b_0 & b_1 & 0 & \ldots & 0 \\
0 & \ddots & \ddots & \ddots & & \vdots \\
\vdots & & \ddots & \ddots & \ddots & 0 \\
0 & & & \ddots & \ddots & b_1 \\
b_1 & 0 & \ldots & 0 & b_{-1} & b_0
\end{bmatrix}.
$$

Further let

$$
T = \begin{bmatrix} A & B \\ B^* & A^* \end{bmatrix},
$$

where X^* stands for the conjugate-transpose of X. Then, the eigenvalues of T are

$$
\lambda_{j,\pm} = \Re\mu_j \pm \sqrt{|\nu_j|^2 - |\Im\mu_j|^2} \in \mathbb{C}, \tag{3.6}
$$

where

$$
\mu_j = a_0 + a_1 e^{\frac{2\pi i j}{J}} + a_{-1} e^{-\frac{2\pi i j}{J}}, \quad \nu_j = b_0 + b_1 e^{\frac{2\pi i j}{J}} + b_{-1} e^{-\frac{2\pi i j}{J}}, \quad j = 1, \ldots, J. \tag{3.7}
$$

Proof. The circulant matrices A and B have the Fourier basis as eigenvectors. Indeed, let $\mathbf{e}_j$ be the vector with entries $\mathbf{e}_{j\ell} = e^{\frac{2\pi i \ell j}{J}}$, where $1 \leq \ell \leq J$ is fixed. Then,

$$
(A\mathbf{e}_j)_\ell = a_0 e^{\frac{2\pi i \ell j}{J}} + a_1 e^{\frac{2\pi i (\ell+1) j}{J}} + a_{-1} e^{\frac{2\pi i (\ell-1) j}{J}}
$$

$$
= e^{\frac{2\pi i \ell j}{J}} \left(a_0 + a_1 e^{\frac{2\pi i j}{J}} + a_{-1} e^{\frac{-2\pi i j}{J}} \right),
$$

and a similar argument holds for B. Hence, $A\mathbf{e}_j = \mathbf{e}_j \mu_j$ and $B\mathbf{e}_j = \mathbf{e}_j \nu_j$. Let F be the discrete Fourier transform matrix with entries $F_{\ell j} = \frac{1}{\sqrt{J}} e^{\frac{2\pi i \ell j}{J}}$, for $\ell, j = 1, 2, \ldots, J$. Then consider the matrix

$$
U = \begin{bmatrix} F & 0 \\ 0 & F \end{bmatrix}^{-1} T \begin{bmatrix} F & 0 \\ 0 & F \end{bmatrix}.
$$

Then, U and T have the same spectrum, and

$$
U = \begin{bmatrix} M & N \\ N^* & M^* \end{bmatrix},
$$

where $M = diag(\mu_1, \ldots, \mu_J)$ and $N = diag(\nu_1, \ldots, \nu_J)$ are diagonal matrices, and μ_j, ν_j are given in (3.7).

The $2J \times 2J$ matrix T operates on $2J$ dimensional vectors, say of the form $(\alpha_1, \ldots, \alpha_J, \beta_1, \ldots, \beta_J)^T$. Now consider the permutation matrix P defined by

$$
P \begin{bmatrix} \alpha_1 \\ \vdots \\ \alpha_J \\ \beta_1 \\ \vdots \\ \beta_J \end{bmatrix} = \begin{bmatrix} \alpha_1 \\ \beta_1 \\ \alpha_2 \\ \beta_2 \\ \vdots \\ \alpha_J \\ \beta_J \end{bmatrix}
$$

Then, $V = PUP^{-1}$ is block diagonal and

$$
V = \begin{bmatrix}
\mu_1 & \nu_1 & 0 & 0 & \ldots & 0 \\
\bar{\nu}_1 & \bar{\mu}_1 & 0 & 0 & \ldots & 0 \\
0 & 0 & \mu_2 & \nu_2 & \ldots & 0 \\
0 & 0 & \bar{\nu}_2 & \bar{\mu}_2 & \ldots & 0 \\
\vdots & & & & \ddots & \ddots \\
0 & \ldots & & 0 & \mu_J & \nu_J \\
0 & \ldots & & 0 & \bar{\nu}_J & \bar{\mu}_J
\end{bmatrix}
$$

The eigenvalues of the diagonal blocks are given by (3.6). $\square$

The following corollary will be used in the computation of the spectral radius of the iteration matrix.

COROLLARY 3.8. *Let A, B and T be as in Lemma 3.7. Let $a_0 = b_0 = 0$, and $a_1, a_{-1}, b_1, b_{-1} \in \mathbb{R}$ be such that*

$$a_1 a_{-1} = b_1 b_{-1}. \tag{3.8}$$

Then,

$$\rho(T) \leq |a_1 + a_{-1}| + |b_1 + b_{-1}|. \tag{3.9}$$

This estimate is sharp: equality in (3.9) holds when J is even, or in the limit when J tends to infinity.

Proof. For convenience, define

$$s_1 = a_1 + a_{-1} \text{ and } s_2 = (b_1 - b_{-1})^2 - (a_1 - a_{-1})^2.$$

From (3.7), for $j = 1, \ldots, J$, we have $\nu_j = (b_1 + b_{-1}) \cos t + i(b_1 - b_{-1}) \sin t$ and $\mu_j = (a_1 + a_{-1}) \cos t + i(a_1 - a_{-1}) \sin t$, where $t = 2\pi j/J$. Therefore, it suffices to show that

$$\phi(t) = (a_1 + a_{-1}) \cos t + \sqrt{(b_1 + b_{-1})^2 \cos^2 t + (b_1 - b_{-1})^2 \sin^2 t - (a_1 - a_{-1})^2 \sin^2 t}$$

$$= (a_1 + a_{-1}) \cos t + \sqrt{(b_1 - b_{-1})^2 - (a_1 - a_{-1})^2 + ((a_1 - a_{-1})^2 + 4 b_1 b_{-1}) \cos^2 t}$$

$$\stackrel{(3.8)}{=} s_1 \cos t + \sqrt{s_2 + s_1^2 \cos^2 t}$$

attains its maximum absolute value when $t = 0$. This follows from the fact that the function $\phi(z) = s_1 z + \sqrt{s_2 + s_1^2 z^2}$, with z in the interval $[-1, 1]$, attains a maximum absolute value of (3.9) either at $z = 1$ or $z = -1$.

The discriminant $d(z) = s_2 + s_1^2 z^2$ is a convex quadratic polynomial, with its minimum at $z = 0$, and is symmetric about $z = 0$ (i.e., $d(z)$ is an even function). It is possible that $d(0) < 0$, however $d(\pm 1) = (b_1 + b_{-1})^2 \geq 0$. Hence, $d(z)$ is non-negative for z^2 in an interval $[\eta^2, 1]$ (and if $\eta > 0$, then $d(z) < 0$ in $(-\eta, \eta)$). Since $\phi(z)$ is real and monotonic on $[-1, -\eta]$ and $[\eta, 1]$, no z in $(-1, -\eta)$ and $(\eta, 1)$ is a global extremum.

If the discriminant $s_2 + s_1^2 z^2$ is non-positive (and in particular, $(\Im \sqrt{s_2 + s_1^2 z^2})^2 = -(s_2 + s_1^2 z^2)$) for z in some interval $[-\eta, \eta]$, then on that interval, we have

$$|\phi(z)| = \sqrt{(\Re\phi(z))^2 + (\Im\phi(z))^2} = \sqrt{(s_1 z)^2 - (s_2 + s_1^2 z^2)} = \sqrt{|s_2|} = \sqrt{|(b_1 - b_{-1})^2 - (a_1 - a_{-1})^2|}$$

$$\leq |a_1 + a_{-1}| + |b_1 + b_{-1}| = \max\{\phi(-1), \phi(1)\}.$$

7

Hence, there is no global maximum in $[-\eta, \eta]$.

To show that equality holds in (3.9) when J is even, observe that $z = 1$ is obtained precisely when $j = 0$, and $z = -1$ is obtained precisely when $j = J/2$. Similarly, if $J \to \infty$, then setting $j = \lfloor J/2 \rfloor$ leads to $z \to -1$. Hence, $\max |\lambda_{j,\pm}| \to \max\{\phi(-1), \phi(1)\}$. $\square$

3.2. Convergence factor of the overlapping algorithm for a general Robin parameter. Using Lemma 3.7 and Corollary 3.8, it is now possible to obtain an estimate for the convergence factor of the iteration. The convergence factor depends on k, the frequency parameter on the fine grid, but also on the parameter $j \in \{1, \ldots, J\}$, which can be interpreted as a frequency parameter for the coarse grid problem.

The proof of the following result is highly technical and it is presented in the Appendix.

LEMMA 3.9. *Consider the CO0 algorithm with J subdomains. An upper bound for the convergence factor for frequencies $k \geq \pi/H$ is*

$$\rho_{p,L,H}(k) = \max_{\pm} |\rho_{p,L,H,\pm}(k)| = \max_{\pm} \left| \frac{-e^{-k\,L}\,(-p+k)^2 + e^{k\,L}\,(p+k)^2 \pm (-p^2+k^2)\,(e^{k\,H} - e^{-k\,H})}{e^{k\,(H+L)}\,(p+k)^2 - e^{-k\,(H+L)}\,(p-k)^2} \right|. \tag{3.10}$$

Further let

$$a_{-1} = a_{-1}(k,p,L,H) = e^{-\frac{1}{2}k\,(H+L)} \left(-2\,(-p+k)^2\,H e^{-\frac{1}{2}k\,(-H+L)} - (-p+k)\,(pH+pL+2) \right)/d, \tag{3.11}$$

$$b_{-1} = b_{-1}(k,p,L,H) = e^{-\frac{1}{2}k\,(H+L)} \left(2\,(-p+k)\,H\,(p+k)\,e^{\frac{1}{2}k\,(-H+L)} - (-p+k)\,(pH+pL+2) \right)/d, \tag{3.12}$$

$$a_0 = a_0(k,p,L,H) = b_0 = b_0(k,p,L,H) = (-pH+pL+2)/d, \tag{3.13}$$

$$a_1 = a_1(k,p,L,H) = e^{\frac{1}{2}k\,(H+L)} \left(-(p+k)\,(-2\,pH - 2\,k\,H)\,e^{\frac{1}{2}k\,(-H+L)} - (p+k)\,(pH+pL+2) \right)/d, \tag{3.14}$$

$$b_1 = b_1(k,p,L,H) = e^{\frac{1}{2}k\,(H+L)} \left(2\,(p+k)\,H\,(-p+k)\,e^{-\frac{1}{2}k\,(-H+L)} + (p+k)\,(pH+pL+2) \right)/d; \tag{3.15}$$

where the denominator d is

$$d = d(k,p,L,H) = -2\,(p+k)^2\,H e^{k\,(H+L)} + 2\,(-p+k)^2\,H e^{-k\,(H+L)}. \tag{3.16}$$

Then, an upper bound for the convergence factor for frequencies $k < \pi/H$ is

$$\rho_{p,L,H}(k) = \max\{|\lambda_{k,1,+}|, |\lambda_{k,1,-}|, |\lambda_{k,-1,+}|, |\lambda_{k,-1,-}|, \Re\sqrt{p_k(1)}, \Re\sqrt{p_k(-1)}\}, \tag{3.17}$$

where $\lambda_{k,\cdot,\cdot}$ and $p_k(z)$ are defined by

$$\lambda_{k,1,\pm} = \lambda_{k,1,\pm}(p,L,H) = (a_0 + a_1 + a_{-1}) \pm (b_0 + b_1 + b_{-1}), \tag{3.18}$$

$$\lambda_{k,-1,\pm} = \lambda_{k,-1,\pm}(p,L,H) = (a_0 - a_1 - a_{-1}) \pm (b_0 - b_1 - b_{-1}), \tag{3.19}$$

$$p_k(z) = p_k(z,p,L,H) = 2(a_0(a_1 + a_{-1}) - b_0(b_1 + b_{-1}))z + a_0^2 + a_1^2 + a_{-1}^2 - b_0^2 - b_1^2 - b_{-1}^2. \tag{3.20}$$

Lemma 3.9 is the first of several technical results. The estimate (3.10) arises naturally from the definition of the iteration and from the formula (3.1) combined with Corollary 3.8. In principle, the low frequency estimate (3.17) is obtained in a similar fashion, but the combination of the local solves with the effect of the coarse grid makes the estimate (3.17) much more complicated.

3.3. Asymptotic convergence factor and the optimized parameter. Given the convergence factor estimate calculated in Lemma 3.9, we can now estimate the asymptotic convergence factor for the Robin parameter $p = p_c^*$ given by equation (3.3). This analysis is technical, so we split it into two lemmas, the first for the high frequencies, and the second for the low, coarse-grid-corrected frequencies. The proofs themselves are in the Appendix.

8

LEMMA 3.10. *Consider the CO0 algorithm with J subdomains, coarse grid parameter H, and overlap parameter L. Fix $c > 0$, let $\epsilon = L/H$ and $p = c\epsilon^{2/3}L^{-1}$. When ϵ is sufficiently small, the convergence factor for frequencies $k \geq \pi/H$ is*

$$\sup_{k \geq \pi/H} \rho(k) = 1 - \min\left\{2\frac{\pi\,(-1+e^{\pi})}{c\,(e^{\pi}+1)}, \sqrt{8c}\right\}\epsilon^{1/3} + O(\epsilon^{2/3}). \tag{3.21}$$

LEMMA 3.11. *Consider the CO0 algorithm with J subdomains, a coarse grid parameter H and an overlap parameter L. Fix $c > 0$. Let $\epsilon = L/H$ and $p = c\epsilon^{2/3}/L$. If ϵ is sufficiently small, the CO0 algorithm converges for frequencies $k < \pi/H$. An upper bound of the asymptotic convergence factor, as $\epsilon \to 0$, is given by*

$$\rho = 1 - \frac{2}{c}\epsilon^{1/3} + O(\epsilon^{2/3}). \tag{3.22}$$

After these two lemmas, all that remains is to put them together and obtain the proof of the main result of this section.

Proof of Theorem 3.1. Putting together (3.21) and (3.22), one obtains (3.4).

For the divergence result, one can verify that

$$\lim_{k \to 0+} \lambda_{k,-1,+}(p, L, H) = (L/H) + 2/(pH) - 1 \geq -1.$$

This is a monotonically decreasing function of p and

$$\lim_{k \to 0+} \lambda_{k,-1,+}(p, L, H) > 1 \text{ when } p < \frac{2}{2H - L},$$

which is (3.5). If the number of subdomains J is even, the value $\lambda_{k,-1,+}(p, L, H)$ is an exact eigenvalue of the iteration matrix $T = T_k$, with $k = 0$, obtained by taking $j = J/2$ in (3.7) and $\lambda_{j,-}$ in (3.6), hence the convergence factor $\rho(T_0) > 1$ (i.e., the iteration diverges for low frequencies[5]), if $p < \frac{2}{2H-L}$. Similarly, if $J \to \infty$ is odd but large, we use $j = \lfloor J/2 \rfloor$ and obtain that $\lambda_{0,z,+} \to \lambda_{0,-1,+}$, cf. (10.3) in the Appendix. □

4. Analysis of the nonoverlapping CO0 algorithm. In addition to the overlapping method analyzed in the previous section, we present a nonoverlapping method here. By setting $L = 0$ in the iteration (2.4), a nonoverlapping, coarse-grid corrected Optimized Schwarz Method is obtained. The optimized Robin parameter for the overlapping algorithm depends on the overlap L and the coarse grid parameter H, but not on the fine grid parameter h. The nonoverlapping optimized Robin parameter also depends on the coarse grid parameter H, but, in addition, it also depends on the fine grid parameter h.

Our analysis of the nonoverlapping algorithm recycles many of the results of the preceding section, and again the technical proofs are detailed in the Appendix. In this section, $L = 0$ (we have a nonoverlapping algorithm), and h is the fine grid size. We define $\epsilon = h/H$, the ratio of the fine grid to the coarse grid parameter.

The estimate (3.10) for the convergence factor for the high frequencies remains valid (if we replace $L = 0$), but now we have that $\lim_{k \to \infty} \rho_{p,0,H}(k) = 1$, which would indicate that the convergence factor is 1, i.e., there is no convergence. To resolve this difficulty, we exploit the fact that the fine grid cannot resolve arbitrarily large frequencies. Indeed, we assume that the fine grid is "semispectral", and that it only resolves frequencies $k < \pi/h$.[6] The convergence factor is then $\rho = \sup_{0 < k < \pi/h} \rho_{p,0,H}(k)$, with $\rho_{p,0,H}(k)$ defined by (3.10) for the high frequencies $k \geq \pi/H$, and by (3.17) for the low frequencies $k < \pi/H$.

---

[5]The frequency $k = 0$ is not part of our spectrum $(\pi/a)\mathbb{N}$, but it is approached when a tends to infinity.

[6]This can be implemented exactly by considering (2.2) and replacing Δv_j^n by $D_{xx}\hat{v}_j^n - k^2\hat{v}_j^n$, etc..., and truncating the Fourier coefficients at $k < \pi/h$. However, a realistic code will typically deviate from this "pure" model by solving the 1d boundary value problems inexactly and even by using a non-spectral scheme in the y direction. This type of analysis, where the model problem studied has some discrete features and some continuous features, is known as a "semidiscrete analysis". The idea of using Fourier transforms in y, even though this may not correspond exactly to the numerical solver, has a long tradition in this field [16].

THEOREM 4.1. *Let $H > 0$ be the coarse grid parameter, and let $0 < h < H$ be the fine grid parameter, with each subdomain having a width of H. Let $J \in \mathbb{N}$ be the number of subdomains. When h/H is small, the optimized parameter of the coarse grid corrected algorithm CO0 is*

$$p_{c,0}^* = c(hH)^{-1/2}.$$

When h/H is small, the convergence factor obtained is

$$\rho(h, H) = 1 - \min\{2/c, 2c/\pi\}(h/H)^{1/2} + O(h/H) < 1. \tag{4.1}$$

Furthermore, the iteration diverges if $p < 1/H$.

REMARK 4.2. *As Theorem 3.1 did for the overlapping iteration, Theorem 4.1 states that the nonoverlapping iteration diverges if p is too small. In order to guarantee $p > 1/H$ regardless of the parameters h, H, ϵ, J, a, one should choose $c > 1$. Note also that as in Remark 3.6, the coefficient $p_{c,0}^*$ is related to the coefficient obtained in [15] for the nonoverlapping case. Also as in Theorem 3.1, the estimate (4.1) only depends on the quotient $\epsilon = h/H$, and not on the specific values of h/H. This is important in the situation where we make h tend to zero, while keeping the quotient $\epsilon = h/H$ constant by increasing the number of subdomains. Such an algorithm scales "weakly".*

5. On the performance of two-level domain decomposition with minimal overlap.

Since the structure for a parallel elliptic solver is sufficiently complicated, it is not immediately obvious that there is a benefit to using an algorithm with a convergence factor of $\rho_{CO0} = 1 - C\epsilon^{1/3}$ (e.g., CO0) over one that has a convergence factor of $\rho_{CS} = 1 - C\epsilon$ (such as Classical Schwarz). In this section, we briefly discuss a simple computational scenario which illustrates the fact that indeed it may be worthwhile to use the method which is in theory asymptotically faster.

We keep the algorithm as simple as possible even though there are many obvious possibilities for improvements. In our scenario, we assume a cluster with a sufficiently large number of processing units, and we calculate the total running time as a function of the fine grid parameter h. Each processing unit handles a single subdomain. In this algorithm sketch, we take an example domain which is a unit square.[7] In this analysis, we further assume that the subdomains are squares of side H, and that the coarse grid has one degree of freedom per subdomain. These dimensions are used to estimate the number of subdomains and elements, but these estimates would be similar if the domain were a more general planar region.

We assume that we want a solution within a tolerance of γh^2, where h is the fine grid size and $\gamma > 0$ is some threshold. This requirement is inspired by the fact that piecewise linear finite element solvers often yield a precision of $O(h^2)$. In two dimensions, we therefore have approximately $m = 1/h^2$ grid points. For simplicity, we choose $L = h$, so that there is one grid length of overlap for all the subdomains. We then choose some coarse grid size H (and thus our subdomain diameters are $H + h$). There are $J = (1/H)^2$ subdomains and consequently each subdomain contains approximately $m' = H^2/h^2$ grid points.

If we assume that multigrid is used for the subdomain solvers, then each local solver can attain a fixed tolerance with $O(m')$ calculations. The number of iterations (or V-cycles) needed to obtain the tolerance γh^2 would then be of the order of $\log(\gamma h^2)$, and thus a local solve would require $C_{loc} = -K \log(\gamma h^2)m'$ calculations.

Once all the local solves have been performed, the local solutions are projected to the coarse grid, and the information is sent to a central server. This central server must now solve an elliptic problem with grid size H, i.e., with $1/H^2$ grid points. This calculation is also performed using a multigrid approach, and the running time is $C_{cg} = -K \log(\gamma H^2)/H^2$. During this time, the rest of the computers in the cluster are idle. Once the coarse grid correction is computed, then it is distributed to all the computers in the network and parallel computation resumes.

The running time for a single iteration (of either CO0 or Classical Schwarz) is $C_{cg} + C_{loc}$. The number of iterations N_{CO0} of CO0 to obtain an error of γh^2 is approximately given by solving $(\rho_{CO0})^{N_{CO0}} = \gamma h^2$, and the total running time until the final stopping criterion is reached is $C_{CO0} = N_{CO0}(C_{cg} + C_{loc})$. We can

---

[7]Our theoretical results in Sections 3 and 4 concern a cylindrical domain, while we are considering here a square domain. We will see (by numerical experiments) in Sections 7 and 8 that the theoretical results also apply to this square domain with square subdomains and cross points.

find the optimal value of ϵ to minimize the running time, and we find that

$$\epsilon_{CO0} \sim 1.29 h^{1/2}, \quad \text{and for this value}$$

$$C_{CO0} \sim -0.11 \frac{\left(7.20 - 14.0 \ln\left(\gamma\, h\right) - 5.0 \ln\left(\gamma\, h^2\right)\right) \ln\left(\gamma\, h^2\right) K}{h^{7/6} C}.$$

Neglecting the polylogarithmic terms, we obtain $C_{CO0} = O(h^{-7/6})$ or $O(m^{0.56333...})$. A similar analysis for the Classical Schwarz iteration with coarse grid correction yields $\epsilon_{CS} \approx 1.57 h^{1/2}$ and $C_{CS} = O(h^{-3/2})$ or $C_{CS} = O(m^{0.75})$ (up to polylogarithmic terms). We see that the best choice of ϵ in both cases ensures that the local problems and the coarse problem have similar numbers of degrees of freedom, so the time spent in the parallel step is proportional to the time spent in the coarse (sequential) step. These results are summarized in Table 5.1.

Note that if we had a Schwarz-like iteration whose convergence factor was independent of ϵ, we would obtain an $O(m^{0.5})$ algorithm, by spending approximately the same amount of time in the parallel code as in the coarse grid correction. This corresponds to the entry marked "Best Possible" in Table 5.1.

<div align="center">

TABLE 5.1

Running times for two-level algorithms (in 2D, m grid points), up to polylogarithmic terms.

Method	Running time
"Best possible"	$O(m^{0.5})$
CO0	$O(m^{0.56333...})$
Classical Schwarz	$O(m^{0.75})$
Sequential multigrid code	$O(m)$

</div>

In our analysis, we have considered a domain decomposition of a cylinder into strips. As a result, when there are many subdomains, there is an unusual anisotropy in the geometry. This does not pose a problem because our coarse grid is designed to handle this anisotropy. Indeed, the grid has one "point" per subdomain in the x direction (and hence these points are "H apart"). These widths are skinny next to the height a of the cylinder, but this is not an issue since the coarse grid has many frequencies in the y direction, corresponding roughly to the "accuracy" of H in the x direction.

That being said, a realistic implementation will use more evenly shaped subdomains, which will introduce cross-points. Although we have not analyzed this version of the algorithm, we will now explain how the algorithm with cross-points is implemented. We will also provide numerical experiments to show that the algorithm with cross-points behaves approximately like the algorithm that we did analyze, which subdivides a cylindrical domain into strips.

6. Implementation of the overlapping CO0 algorithm. The algorithm we have analyzed is specific to the Laplacian on the cylinder, where the subdomains are strips. Nevertheless, our CO0 method is applicable to more general domains and subdomains. We now introduce a variant which we can use for general domains, and we demonstrate in Sections 7 and 8 with numerical experiments that our optimized parameter (3.3) gives good convergence results when applied to these more general situations.

In [13], [42] it is shown that, under certain conditions, the Classical Schwarz and Optimized Schwarz algorithms converge at the same rate as the Restricted Additive Schwarz (RAS) and Optimized Restricted Additive Schwarz (ORAS) variants, respectively; RAS was introduced in [5], and analyzed in [14]. In a Schwarz iteration that also includes a coarse grid correction, it is therefore possible to implement the local solves using a RAS approach, but the coarse grid correction must be treated separately (and "multiplicatively"), because it overlaps with all of the subdomains. We now discuss such an implementation for overlapping subdomains.

6.1. Components of Restricted Additive Schwarz (RAS). Let Ω be the domain and $\Omega_1, \ldots, \Omega_J$ be the subdomains, and let $\Gamma = \Omega \cap (\cup_j \partial \Omega_j)$ (the "interface"). We denote by $\mathbf{x}_1, \ldots, \mathbf{x}_m$ the nodes of the triangulation τ of Ω (or of the grid), *excluding those nodes on the boundary* $\partial \Omega$. When using a piecewise linear finite element discretization, one obtains the $m \times m$ stiffness matrix A of the Laplacian on Ω, with entries given by

$$A_{ij} = \int_\Omega \nabla \phi_i \cdot \nabla \phi_j,$$

where ϕ_i and ϕ_j are piecewise linear functions on τ, where as usual

$$\phi_k(\mathbf{x}_\ell) = \begin{cases} 0 & \text{if } k \neq \ell, \\ 1 & \text{if } k = \ell. \end{cases}$$

Each subdomain Ω_j, $j = 1, \ldots, J$, contains m_j vertices $\mathbf{x}_{j,1}, \ldots, \mathbf{x}_{j,m_j}$, *including those on* $\partial\Omega_j \cap \Omega$. Some of these vertices are "interior" (they are in Ω_j), and some of the vertices are on the interface $\partial\Omega_j \cap \Omega$. For each subdomain Ω_j, we can define an $m_j \times m$ restriction matrix R_j, whose entries are zeroes and ones, by:

$$(R_j)_{k,\ell} = \begin{cases} 1 & \text{if } \mathbf{x}_{j,k} = \mathbf{x}_\ell, \\ 0 & \text{otherwise.} \end{cases}$$

We can think of the matrix R_j as mapping a finite element function on Ω to its restriction on Ω_j. We can conversely think of R_j^T as a matrix which prolongs a finite element function of Ω_j to all of Ω by padding it with zeroes.

In the RAS method, one further defines matrices $\tilde{R}_1, \ldots, \tilde{R}_J$, where $\tilde{R}_j$ is also $m_j \times m$ and consists of zeroes and ones, in such a way that

$$\sum_{j=1}^{J} \tilde{R}_j^T R_j = I.$$

These restriction matrices usually correspond to a nonoverlapping partition of the unknowns given by a nonoverlapping decomposition $\{\tilde{\Omega}_j\}_{j=1}^{J}$ of Ω. When the domain decomposition has one grid length of overlap, the restrictions $\tilde{R}_j$ can be obtained from R_j by replacing any row corresponding to a vertex on $\partial\Omega_j$ with a zero row.

Given an initial vector $\mathbf{v}^0$, the one-level RAS algorithm is then given by

$$\mathbf{v}^{n+1} = \mathbf{v}^n + \sum_{j=1}^{J} \tilde{R}_j^T A_j^{-1} R_j (\mathbf{f} - A\mathbf{v}^n), \quad n = 0, 1, \ldots, \tag{6.1}$$

where the local matrices are

$$A_j = R_j A R_j^T, \quad j = 1, \ldots, J. \tag{6.2}$$

REMARK 6.1. *Note that our definition of the restriction matrices R_j is slightly different from the usual definition found in the literature on Additive Schwarz preconditioners, since we are keeping unknowns on the interface Γ. The reason behind this choice is that we will impose Robin transmission conditions on this interface, and we will need those unknowns when discretizing the local problems.*

6.2. Coarse spaces. In this section, we define a coarse space by constructing basis functions on a coarse mesh. The resulting coarse space correction will be quite different from the one described in Section 2, but we aim to show with numerical experiments that the results of the convergence analysis still hold for other decompositions and different coarse spaces. Consider, for the purpose of the explanation, the example of a square domain $\Omega = (0, 1) \times (0, 1)$ with 16 overlapping subdomains (4×4 decomposition).

The classical approach for the Additive Schwarz preconditioner is to introduce a coarse mesh as in Figure 6.1(a). Note that the coarse mesh may not conform with the fine mesh when both are required to be uniform; this is how the coarse mesh was implemented in our solver. If we denote the interior nodes of this coarse mesh by $\mathbf{y}_1, \ldots, \mathbf{y}_{m_0}$ (assuming homogeneous Dirichlet boundary condition on $\partial\Omega$), we choose piecewise bilinear hat functions on this coarse mesh

$$\psi_j(\mathbf{y}_k) = \begin{cases} 1 & \text{if } j = k, \\ 0 & \text{otherwise.} \end{cases}$$

To construct the operators on this coarse space, each coarse basis function ψ_j is evaluated at each of the fine mesh nodal points, $\psi_j(\mathbf{x}_\ell)$, $\ell = 1, \ldots, m$. We then store these functions as rows of the $m_0 \times m$ matrix

$$R_0 = \begin{bmatrix} \psi_1(\mathbf{x}_1) & \cdots & \psi_1(\mathbf{x}_m) \\ \vdots & \cdots & \vdots \\ \psi_{m_0}(\mathbf{x}_1) & \cdots & \psi_{m_0}(\mathbf{x}_m) \end{bmatrix}.$$

(a) classical coarse mesh   (b) new coarse mesh

FIG. 6.1. *Two different coarse meshes: the classical version is uniform, whereas the new proposed mesh is better suited to a RAS implementation. The circles indicate degrees of freedom (coarse nodes).*
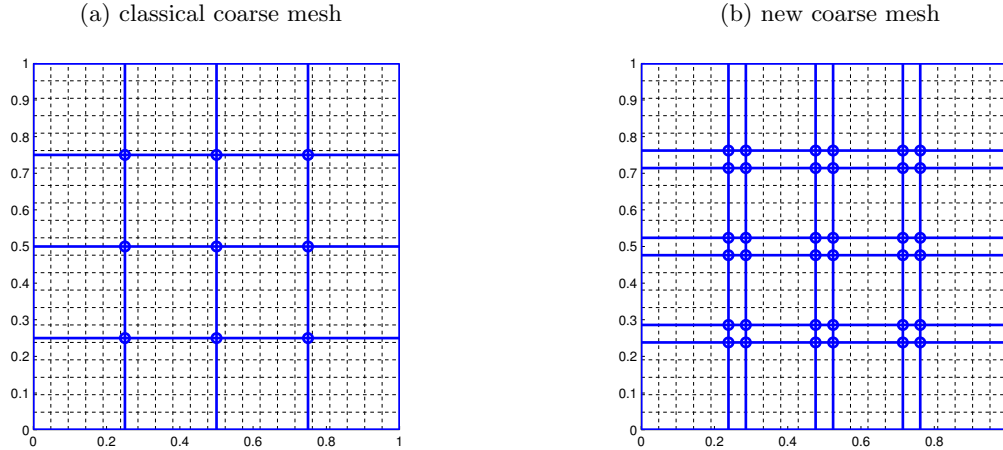
Thus, the matrix R_0^T will be the natural interpolation from the coarse to the fine space, and R_0 will be the associated restriction matrix. The induced coarse matrix is defined by $A_0 = R_0 A R_0^T$.

The coarse mesh described previously performs well for the Additive Schwarz method: if we think of the discrete vectors as functions in space, then the application of Additive Schwarz produces continuous iterates over the domain, so the coarse correction can be smooth. On the other hand, in the RAS method, the subdomain approximations are combined to produce discontinuous iterates, and thus smooth coarse corrections will not be as effective. We now introduce a different coarse space, which we believe is better suited and more efficient when using a RAS implementation. It stems from the observation that, in the one-level RAS iteration (6.1), after the first iteration the residual is always 0 at the interior nodes of each $\tilde{\Omega}_j$. In other words, the residual after each iteration is only nonzero at nodes $\mathbf{x} \in \tilde{\Omega}_j$ that have a neighbor in another partition $\tilde{\Omega}_k$.

To mimic this observation, we pick coarse basis functions that are discrete harmonic in the interior of $\tilde{\Omega}_j$, and can only have nonzero residuals at nodes described above. For our example on the square, this suggests introducing the coarse mesh shown in Figure 6.1(b) and constructing piecewise bilinear basis functions on this mesh instead. Observe that this coarse mesh is completely independent of the size of the overlap, it only depends upon the definition of $\tilde{R}_j$ (the subdomains are not depicted in Figure 6.1). Note also that this coarse space will have $m_0 = 36$ degrees of freedom in our example, four times as many as the classical approach.

6.3. RAS algorithm to solve $A\mathbf{u} = \mathbf{f}$. The one-level RAS iteration is given by (6.1). By treating the coarse space correction "multiplicatively", the two-level RAS algorithm is

$$\mathbf{v}^{n+1/2} = \mathbf{v}^n + \sum_{j=1}^{J} \tilde{R}_j^T A_j^{-1} R_j (\mathbf{f} - A\mathbf{v}^n), \tag{6.3}$$

$$\mathbf{v}^{n+1} = \mathbf{v}^{n+1/2} + R_0^T A_0^{-1} R_0 (\mathbf{f} - A\mathbf{v}^{n+1/2}), \tag{6.4}$$

where

$$A_j = R_j A R_j^T, \quad j = 0, 1, \ldots, J.$$

To obtain faster convergence, we can use a Krylov subspace method such as GMRES with the two-level RAS as the preconditioner (which is nonsymmetric in this case).

6.4. ORAS algorithm to solve $A\mathbf{u} = \mathbf{f}$. In [42], the Optimized Restricted Additive Schwarz (ORAS) algorithm was introduced. It is easily obtained by replacing the local matrices A_j with matrices $\tilde{A}_j$ corre-

sponding to the discretization of the local problem on subdomain Ω_j with Robin boundary condition

$$\frac{\partial u_j}{\partial n_j} + p u_j = 0 \qquad \text{on } \partial\Omega_j \backslash \partial\Omega.$$

Because this is only a change in the interface condition, the local matrices only need to be modified for unknowns on, and possibly near, the interface Γ. Of course, this modification depends on the discretization of the problem and may not be unique.

Given an initial vector $\mathbf{v}^0$, the one-level ORAS algorithm is

$$\mathbf{v}^{n+1} = \mathbf{v}^n + \sum_{j=1}^{J} \tilde{R}_j^T \tilde{A}_j^{-1} R_j (\mathbf{f} - A\mathbf{v}^n), \tag{6.5}$$

and the two-level ORAS iteration is given by

$$\mathbf{v}^{n+1/2} = \mathbf{v}^n + \sum_{j=1}^{J} \tilde{R}_j^T \tilde{A}_j^{-1} R_j (\mathbf{f} - A\mathbf{v}^n), \tag{6.6}$$

$$\mathbf{v}^{n+1} = \mathbf{v}^{n+1/2} + R_0^T A_0^{-1} R_0 (\mathbf{f} - A\mathbf{v}^{n+1/2}). \tag{6.7}$$

Two important remarks need to be made here. First of all, the "physical" overlap is different in the RAS and ORAS methods. From the way we have defined RAS, the Dirichlet interface conditions are *not* imposed on Γ: the local matrices A_j correspond to having $u = 0$ at the nodes *outside* Ω_j, because Ω_j includes the nodes on its boundary. Thus, the physical overlap of RAS has two additional mesh layers when compared to ORAS. We will use L to denote the overlap width in the ORAS algorithm, and it should be understood that the RAS algorithm has a wider physical overlap of $L + 2h$. On the other hand, the "algebraic" overlap between the discrete degrees of freedom is the same for both methods.

The second remark concerns the equivalence between the one-level ORAS (6.5) and a Schwarz iteration on the subdomains of the form

$$\tilde{A}_j \mathbf{v}_j^{n+1} = \mathbf{f}_j + \sum_{j=1}^{J} \tilde{B}_{jk} \mathbf{v}_k^n, \quad j = 1, 2, \ldots, J, \tag{6.8}$$

where $\tilde{B}_{jk}$ perform the extraction of interface conditions from neighboring subdomains; see [42] for details. It is shown in [42] that such an equivalence holds under certain conditions. For a decomposition into strips, these conditions amount to having enough overlap: in our notation, $L = h$ is sufficient to satisfy these conditions. However, when there are crosspoints (as in Figure 6.1), an algebraic condition given in [42] becomes more restrictive. In [11], it is shown that for Robin conditions, it is sufficient in the presence of crosspoints to use a first order accurate discretization of the normal derivative for the equivalence to hold. One may decide to apply ORAS regardless of whether equivalence holds or not, however the convergence behavior may not be as expected, and the choice of the optimized Robin parameter may also be affected, since the analysis of optimized Schwarz methods is usually done for the continuous analogue of iteration (6.8).

7. Numerical experiments with overlapping subdomains. Throughout this section, we consider overlapping subdomains and we use the RAS and ORAS implementations discussed in Section 6. We consider the unit square $\Omega = (0, 1) \times (0, 1)$ decomposed uniformly into J subdomains with $L = h$ (minimal overlap). We solve the problem $-\Delta u = f$ with homogeneous Dirichlet boundary conditions, discretized using the standard 5-point finite difference stencil.[8] To obtain the local matrices $\tilde{A}_j$, we use only a *first-order* accurate discretization of the normal derivative in the Robin conditions; this implies that we need only to modify diagonal entries from A_j for the unknowns on the interface, and thus we are able to satisfy the equivalence conditions of [42]. The coarse space is still constructed from bilinear basis functions on a coarse mesh. For the one-level and two-level ORAS methods, we use the Robin parameters given by the formulas

$$p^*_{\text{one-level}} = 2^{-1/3} \pi^{2/3} h^{-1/3} \approx 1.7 h^{-1/3}, \tag{7.1}$$

$$p^*_{\text{two-level}} = 2^{-1/3} \pi^{2/3} h^{-1/3} H^{-2/3} \approx 1.7 h^{-1/3} H^{-2/3}, \tag{7.2}$$

---

[8]This is a problem that is very similar to the one treated in [15] and several other places, but our experiments include a coarse grid correction that gives good scaling properties.

FIG. 7.1. *Convergence as we refine h for the different iterative methods, on a unit square with 16 subdomains.*
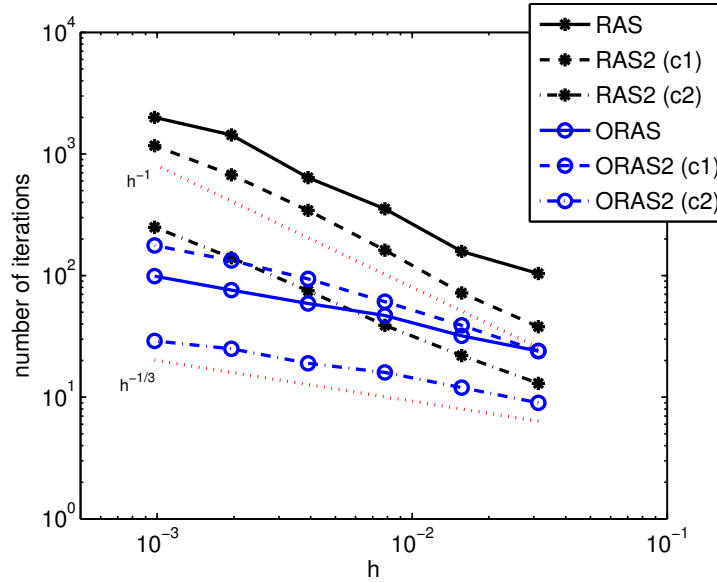
cf. (3.3).

For the iterative applications of RAS (6.3)-(6.4) and ORAS (6.6)-(6.7), we measure the relative error in the supremum norm on Ω. For the preconditioned GMRES method (without restart), the convergence is measured with the relative ℓ_2-norm of the residual. We report the number of iterations when the error falls below a tolerance of 10^{-8}. The results shown were obtained from a parallel code using the library PETSc [2], and running on an Orion cluster of 96 processors.

There are several parameters to vary, and in particular we explore three different relevant cases.

7.1. Decreasing the fine mesh size h. First, we fix the number of subdomains to $J = 16$ (4×4 decomposition). Recall that we choose the minimal overlap $L = h$. The results for the iterative application of the algorithms are illustrated in Figure 7.1. The labels RAS and ORAS refer to the one-level methods, whereas RAS2 and ORAS2 refer to the two-level versions with coarse space correction. We compare the two choices of the coarse mesh: the classical mesh from Figure 6.1(a) is denoted by (c1) and the new coarse mesh from Figure 6.1(b) by (c2).

It is clear that the new coarse mesh we propose yields much faster convergence than the classical mesh: when $h = 1/512$, RAS2(c1) and ORAS2(c1) need 674 and 133 iterations to converge, respectively, whereas RAS2(c2) and ORAS2(c2), with the new coarse mesh, require only 140 and 25 iterations, respectively. Of course, some improvement was expected because the new coarse space has four times the dimension of the classical coarse space. However, we believe that the idea of capturing where the residual is nonzero with the new coarse mesh was key in obtaining this significant improvement in convergence.

Figure 7.1 also shows reference lines of slope -1 and $-1/3$. We observe very good agreement with our expectation that one-level and two-level RAS have a convergence factor of the form $\rho \sim 1 - O(h)$, and that one-level and two-level ORAS have the better convergence factor $\rho \sim 1 - O(h^{1/3})$, as the theory predicts. Under GMRES acceleration, the number of iterations for the different preconditioners are listed in Table 7.1. We also find the weaker dependence on $L = h$ for the optimized Robin conditions, both for the one-level and two-level preconditioners. The difference in performance between the two coarse spaces is greatly attenuated by the Krylov subspace method.

7.2. Weak scaling experiment (h/H constant). In our second experiment, we decrease the mesh size h (recall that $L = h$) and increase the number of subdomains J in such a way that the ratio h/H remains constant (see Remark 3.2). To achieve this, we keep the size of the local problems fixed to 256×256, i.e., each processor has a constant number of unknowns, and we use more processors, thus increasing the size of the global problem. This gives the constant ratio $h/H = 1/256 \approx 0.004$. Table 7.2 shows the weak scalability

TABLE 7.1
Number of iterations for the preconditioned GMRES method.

	one-level		two-level (c1)		two-level (c2)	
h	RAS	ORAS	RAS2	ORAS2	RAS2	ORAS2
1/64	30	18	17	14	15	10
1/128	41	20	23	14	20	12
1/256	56	22	31	16	27	15
1/512	72	24	40	18	37	16
1/1024	99	27	52	20	49	19

TABLE 7.2
Number of iterations for a weak scaling experiment, when $h/H \approx 0.004$ is constant.

J	4	16	36	64	81
no. of unknowns	$262,194$	$1,048,576$	$2,359,296$	$4,194,304$	$5,308,416$
	Iterative method				
RAS2	243	250	266	264	271
ORAS2	27	29	31	31	31
	Preconditioned GMRES				
RAS2	45	49	49	50	50
ORAS2	16	19	19	19	19

of the two-level preconditioners (we only use the new coarse mesh here), under both the CO0 iteration (2.4) and its application as a preconditioner to GMRES.

Recall that the dimensions of the local matrices for RAS and ORAS are exactly the same, and that we use the same coarse space for both methods. The cost of modifying the matrices A_j to obtain $\tilde{A}_j$ is negligible. So, the computational cost for constructing and applying the RAS2 and ORAS2 preconditioners is the same. Hence, in this example, under GMRES acceleration, the ORAS2 method is more than twice as fast as the RAS2 preconditioner. This performance improvement will become greater if we increase the size of the local problems (smaller h/H).

7.3. Varying the Robin parameter p. The question arises whether the formula for the optimized Robin parameter (7.2), coming from the analysis, gives a good approximation to the *best* parameter value in practice, and whether the asymptotic behavior of the parameter is correct when h and H are small. In this section, we test several values of the Robin parameter p, and compute in each case an approximation of the convergence factor ρ given by

$$\rho \approx \left(\frac{\text{sup-norm error at iteration } 15}{\text{sup-norm error at iteration } 10} \right)^{1/5}.$$

For the specific problem with $h = 1/512$, $L = h$, and $J = 16$ subdomains, this approximation to ρ is plotted in Figure 7.2 for 100 values of the Robin parameter p. Note that we can get divergence of the iteration when choosing p too small. Also, note that the value obtained from the formula $p^* = 2^{-1/3}\pi^{2/3}h^{-1/3}$ for the one-level method and two subdomains can be significantly less efficient compared to the best numerical value in the case of many subdomains.

Next, we find the best Robin parameter in our solver by minimizing the estimation of ρ over a uniform sample of 100 values of p (this is a very crude optimization procedure). By varying the fine grid size h (with H constant) and the number of subdomains (with h constant) independently, we show in Figure 7.3 that the best Robin parameter for the two-level ORAS iteration has the asymptotic behavior $p \sim O(H^{-2/3}h^{-1/3})$, confirming the result of Theorem 3.1 where the formula $p_c^* = cH^{-2/3}L^{-1/3}$ is found. In general, the best choice for the constant c will depend on the particular discretization and implementation of the method; in this case, we find that $c \approx 1.4$ works better than the value 1.7.

8. Implementation of the nonoverlapping CO0 algorithm. We now present numerical experiments with two different implementations of the nonoverlapping algorithm. The first example implements a

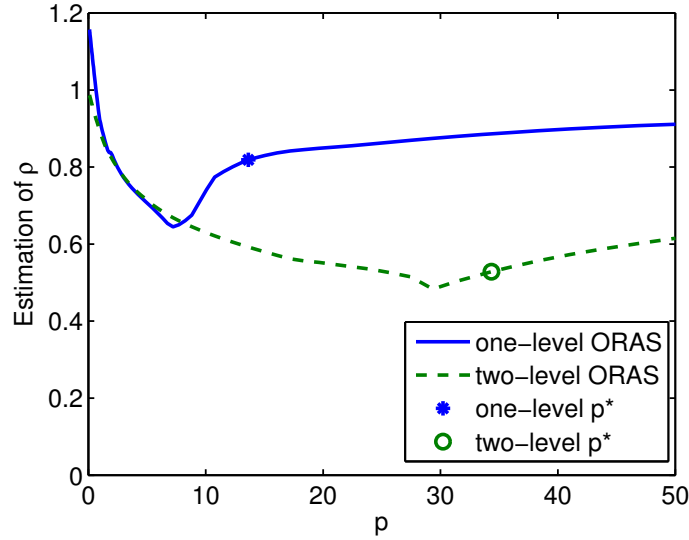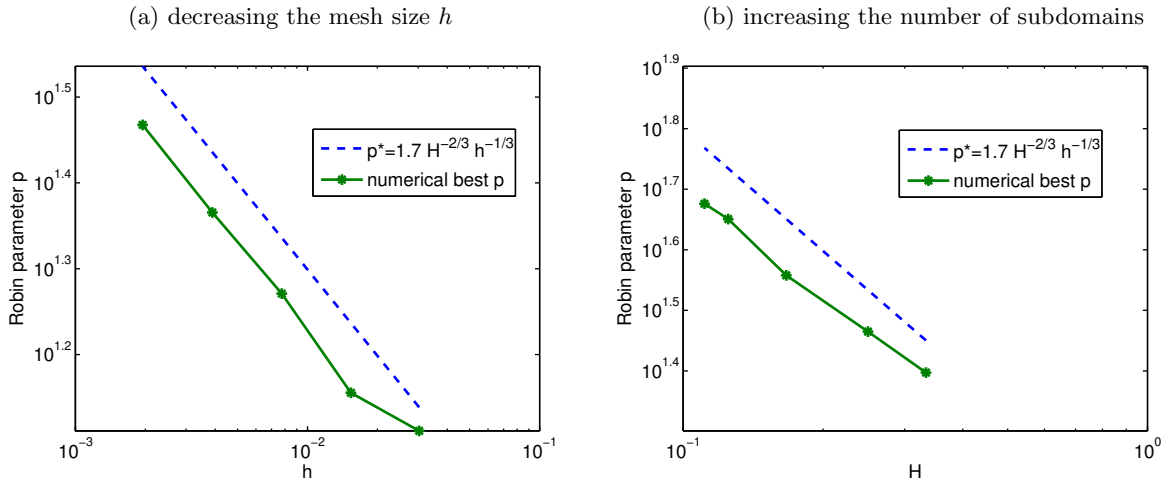FIG. 7.2. *Numerical estimate of the convergence factor for various Robin parameters p.*

FIG. 7.3. *Comparison of the best numerical values of the Robin parameter with the formula p* for two-level ORAS.*

(a) decreasing the mesh size h (b) increasing the number of subdomains

finite element discretization for a decomposition into strips, with a coarse space similar to the one introduced in Section 2 for the convergence analysis. The second implementation consists of spectral elements, with a specific coarse space that will be described. In both cases, the algorithms will use an *augmented* formulation.

8.1. Finite element method. There is no RAS version of the nonoverlapping algorithm, we therefore implemented an iteration on the augmented system. Our domain is the unit square, which we subdivide into J strips along the x axis; each strip has width $H = 1/J$. The nodal values for subdomain Ω_j correspond to the vertices in $[jH, (j + 1)H] \times (0, 1) \cap (0, 1) \times (0, 1)$; i.e., each subdomain Ω_j has degrees of freedom associated with vertices inside Ω_j, or on the artificial interfaces $\partial\Omega_j \cap (0, 1) \times (0, 1)$.

The problem is discretized with bilinear finite elements on the fine mesh. Let N_j be the $m_j \times m_j$ matrix whose entries are

$$(N_j)_{k,\ell} = \int_{\Omega_j} \nabla\phi_{\mathbf{x}_{j,k}} \cdot \nabla\phi_{\mathbf{x}_{j,\ell}},$$

where we have abused the notation and denoted the piecewise linear basis function for vertex $\mathbf{x}_{j,k}$ by $\phi_{\mathbf{x}_{j,k}}$. The matrix N_j is the stiffness matrix for a Neumann problem for the Laplace operator on Ω_j. Likewise, let

17

B_j be the $m_j \times m_j$ matrix whose entries are

$$(B_j)_{k,\ell} = \int_{\partial\Omega_j \cap \Omega} \phi_{\mathbf{x}_{j,k}} \phi_{\mathbf{x}_{j,\ell}}.$$

In this way, the matrix

$$\tilde{A}_j = N_j + pB_j$$

is the stiffness matrix for a Robin problem for the Laplace operator on Ω_j, with Robin parameter p.

In subdomain Ω_j, the iterate $\mathbf{v}_j^{n+1/2}$ is obtained by solving the Robin problem

$$\tilde{A}_j \mathbf{v}_j^{n+1/2} = R_j(\mathbf{f} + \sum_{\ell=j-1,j+1} R_\ell^T (pB_j - N_j)\mathbf{v}_\ell^n).$$

To compute a coarse grid correction, we glue together the local solutions into a single-valued function $v^{n+1/2}$ of the domain $(0,1) \times (0,1)$. If $\mathbf{x}_j = (x_j, y_j)$ is a vertex of the triangulation, and if $\ell H \leq x_j < (\ell+1)H$, then we define $v^{n+1/2}(\mathbf{x}_j) = v_\ell^{n+1/2}(\mathbf{x}_j)$. Given this "reassembled iterate", we can compute a global residual and hence a coarse grid correction.

We define coarse "basis functions" in each subdomain. For subdomain Ω_j, a basis function ψ is linear in x and piecewise linear in y, with nodes at $y = H, 2H, \ldots, (J-1)H$; there are $2(J-1)$ such functions per subdomain. We concatenate the basis vectors for subdomain Ω_j as column vectors to form the matrix Q_j, whose size is $m_j \times 2(J-1)$, where m_j is the number of degrees of freedom for the Robin problem on Ω_j. We let $\bar{Q} = diag(Q_1, \ldots, Q_J)$ and we let $\bar{R}^T = [\tilde{R}_1^T \ldots \tilde{R}_J^T]$. The coarse grid correction matrix is

$$A_0 = (\bar{R}^T \bar{Q})^T A (\bar{R}^T \bar{Q}).$$

We compute the coarse grid correction by solving the linear problem

$$\mathbf{z}^{n+1/2} = \bar{Q} A_0^{-1} \bar{Q}^T \bar{R}(\mathbf{f} - A\mathbf{v}^{n+1/2}).$$

The coarse grid correction to be applied to subdomain Ω_j is now represented in the jth block of coefficients of $\mathbf{z}^{n+1/2}$. To extract those coefficients, we can define a block matrix $C_j = [0 \ldots 0 \ I \ 0 \ldots 0]$, where each 0 block is a $2(J-1) \times 2(J-1)$ zero matrix, and I is the $2(J-1) \times 2(J-1)$ identity. Then, the coarse-grid-corrected iterate is

$$\mathbf{v}_j^{n+1} = \mathbf{v}_j^{n+1/2} + C_j \mathbf{z}^{n+1/2}.$$

We can optionally apply the coarse grid correction to the "reassembled iterate"

$$\mathbf{v}^{n+1} = \bar{R}^T \mathbf{z}^{n+1/2},$$

although this calculation is not used in the computation of $\mathbf{v}_j^{(n+1)+1/2}$.

8.1.1. Numerical results. We have performed a numerical experiment with $J = 4$ subdomains and random initial vectors $\mathbf{v}_1^0, \ldots, \mathbf{v}_J^0$, and report the results in Table 8.1. For h, we use the values $h = 1/16, 1/32, 1/64, 1/128$. We use the optimized Robin parameter $p_{4,0}^* = 4(hH)^{-1/2}$. The coefficient $c = 4$ was found to be a good value numerically. The convergence factor $\rho(h)$ is estimated by the formula $\rho(h) \approx (\|\mathbf{v}^{15} - \mathbf{u}\|_\infty / \|\mathbf{v}^{10} - \mathbf{u}\|_\infty)^{1/5}$, where $\mathbf{u} = A^{-1}\mathbf{f}$ is the true solution. We also give the number of iterations before the relative error, in the uniform norm, is less than 10^{-6}. Observe that going from $h = 1/64$ to $h = 1/128$ increases the iteration count by a factor of 1.25, while the theoretical prediction is $\sqrt{2} \approx 1.4$.

We also have a scaling experiment in the H variable in Figure 8.1. We set $h = \frac{1}{64}$ and we vary $H = \frac{1}{4}, \frac{1}{8}, \frac{1}{16}, \frac{1}{32}$. We run the nonoverlapping CO0 iteration and count the number of iterations before the error is less than the tolerance 10^{-6}. From this experiment, we notice the very good agreement of the scaling properties with the estimate (4.1).

TABLE 8.1
Estimated convergence factors and number of iterations for the nonoverlapping algorithm for various values of h.

h	$\rho(h)$	Iterations
1/16	0.5994	22
1/32	0.6139	26
1/64	0.6576	32
1/128	0.7318	40

FIG. 8.1. *Iteration counts for nonoverlapping CO0 for various values of H.*
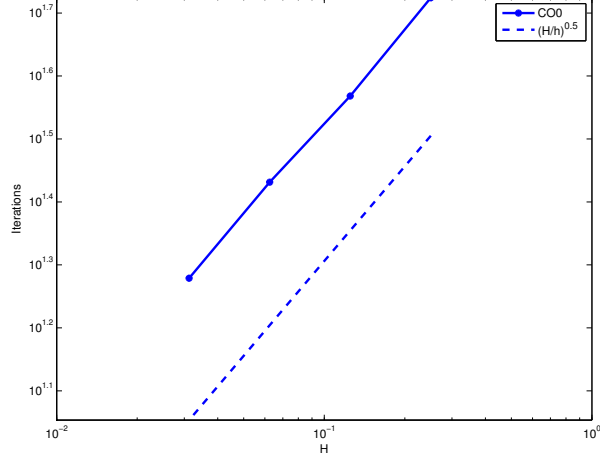
8.2. Spectral element method (SEM).

We now consider the spectral element discretization as introduced by [32], [38]. To that end, we tile the original computational domain Ω into J subdomains Ω_j with $j = 1, 2..., J$ consisting of quadrangles. On each tile, a high-order tensor product Lagrange basis is constructed using the points of the Gauss-Legendre-Lobatto (GLL) quadrature rule. The corresponding space is

$$\mathbf{P}_N = \{v_h \in L^2(\Omega) \mid v_h|_{\Omega_j} \circ T_{\Omega_j} \in (\mathbb{P}_N \otimes \mathbb{P}_N)(\Omega_j) \quad \forall \, \Omega_j \in \mathcal{T}_h \}$$

with T_{Ω_j} the image of the reference element $[-1,1] \times [-1,1]$ for quadrangle Ω_j. With SEM, an augmented system can be built quite naturally and a description of this procedure can be found in [42]. The coarse problem is then constructed by taking advantage of the rich polynomial space. A different polynomial degree M with $M < N$ is chosen over the same mesh $\mathcal{T}_h$. That coarse correction is then applied in a multiplicative fashion as aforementioned.

8.2.1. Numerical experiments.

As a first test, we look at the strip decomposition involved in the development of the theory. We perform tests for various ratios of the fine mesh spacing versus the element width, as well as for three different values of the constant c in the formula $p^*_{c,0} = c(hH)^{-1/2}$ for the Robin parameter. It should be noted in passing that the smallest spacing between the GLL points scales as $h = O(N^{-2})$. Thus doubling the polynomial degree corresponds to dividing the effective h by 4. The theory predicts that dividing h by 4 would lead to twice the number of stationary iterations, or $\sqrt{2}$ times the number of preconditioned Krylov iterations. We observe such a behavior in Table 8.2 when the iterations for $N = 8$ and $N = 16$ are compared. For a constant c too large we observe that this property is lost.

The second test considers a 2D domain with fixed polynomial degrees N and M for the the fine and coarse grid, respectively. The number of elements is increased in both directions and, in this case, our theory predicts that the convergence rate is a function of the ratio $\epsilon = h/H$ which stays constant. Therefore, the number of iterations should be bounded (or reach a fixed value) as the number of subdomains is increased. In this case we use $c = 4$ for the Robin parameter involved in the transmission condition. The number of iterations seems to plateau at 40 GMRES iterations when going from 256 domains to 400. A random starting vector was employed in the experiment as well as bi-periodic boundary conditions. The results are reported in Table 8.3.

FIG. 8.2. *Geopotential height field after 15 days for the flow over the mountain test. The center of the mountain (not depicted), is located at coordinates $(270^o, 30^o)$ in spherical coordinates. The contour regions start from (dark blue) $5100m$ up to $5900m$ (dark red).*
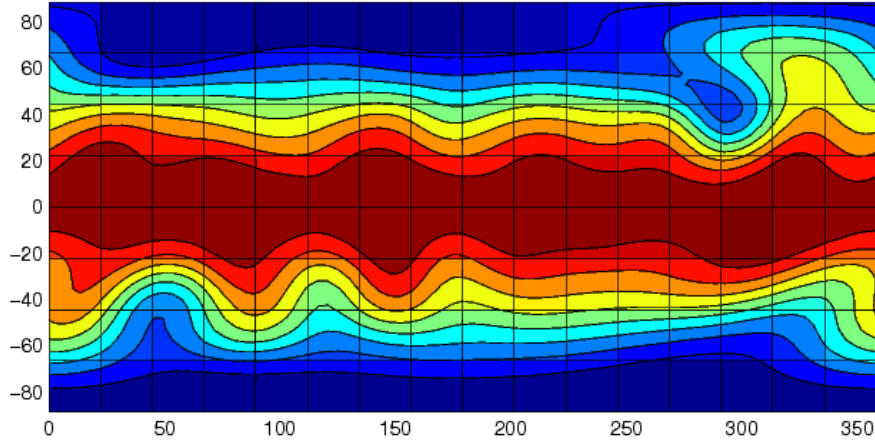

TABLE 8.2
Number of stationary iterations before the error drops below 10^{-6} for increasing number of spectral elements: strip decomposition with 10 elements

	$N = 8$	$N = 10$	$N = 12$	$N = 14$	$N = 16$	$N = 18$
$M = 3, c = 2.0$	17	21	25	30	34	38
$M = 3, c = 2.5$	15	19	25	26	31	34
$M = 3, c = 3.0$	15	19	25	29	35	37

8.3. Shallow water. Finally, we consider an application to the shallow water equations on the sphere. They are traditionally used to investigate promising numerical methods for global numerical climate modeling. The shallow water equations are derived from the Navier-Stokes equations in the case where the horizontal length scale is much larger than the vertical one. This results in three equations: two momentum equations for velocities and one for conservation of the geopotential height[9]. On the sphere, the Coriolis terms are added to the momentum equations. Here we consider the case of the positive definite Helmholtz problem arising either in a semi-implicit semi-Lagrangian (SISL) discretization [43], [44], or as a gravity wave preconditioner for a fully implicit time discretization [41]. In both cases, omitting the details, we are lead to the problem $(\frac{I}{\Delta t^2} - \Delta)u = f$ where Δt can be chosen large enough such that the stiffness of the Laplacian dominates. In this extreme case, we want to observe a plateau in the number of iterations as the number of spectral elements on the sphere is increased. A right hand side is generated from a high-resolution simulation extracted from the high-order methods modeling environment code [4]. Then the problem is solved in latitude-longitude coordinates using zero as a starting vector for GMRES. The shallow water test case we consider consists in a flow impinging a mountain and originally described in [46] as test case 5. As Table 8.4 reports, the number of iterations seems bounded at 29 when $N = 8$ and $M = 3$ for the coarse grid. Thus very efficient time discretizations can be crafted using the CO0 algorithm. A plot of the geopotential height of the solution at day 15 of the simulation is depicted in Figure 8.2.

9. Conclusions. In optimized Schwarz methods (OSM), Robin or higher order transmission conditions are used at the artificial interfaces between subdomains, in order to obtain faster convergence. This is the

---

[9]The geopotential height is the usual height at sea level, multiplied by the gravitational acceleration constant.

TABLE 8.3
Number of GMRES iterations before the error drops below 10^{-10} for increasing number of spectral elements

	2×2	4×4	8×8	12×12	16×16	20×20
$N = 8, M = 3$	24	31	36	38	40	40

TABLE 8.4
Number of GMRES iterations before the error drops below 10^{-10} for increasing number of spectral elements

	4×2	8×4	16×8	24×12
$N = 8,\ M = 3$	24	27	29	29

first paper in which an analysis of (multiplicative) coarse grid correction for OSMs is presented. Our analysis for a model problem (the Laplacian on a cylinder, with the subdomains being overlapping strips and Robin transmission conditions) shows that the eigenvalues of the preconditioned system lie within a disc of radius $1 - O(h/H)^{1/3}$ centered at $z = 1$. This tight clustering of the eigenvalues can be attractive for the convergence of many Krylov subspace methods.

Our new coarse mesh is especially tailored for the discontinuous iterates of OSM, and thus also very suitable for classical RAS implementations. We illustrate this by numerical experiments, and also show that our results for the special case in our analysis seem to hold in the more general setting of arbitrary decompositions.

Acknowledgement. We thank the referees for their questions and suggestions which helped improve our presentation.

10. Appendix. We present in this appendix the four proofs postponed from the body of the paper. Some of the proofs are highly technical. This is unfortunately unavoidable if we want to allow the reader to check the analysis. We attempt to provide some guidance at the beginning of each argument, but the arguments themselves remain challenging.

The four proofs collected in the present appendix are as follows. For the overlapping case, the proof of Lemma 3.9 is an estimate of the convergence factor of the CO0 method for arbitrary Robin parameter p. The estimates for the optimized Robin parameter (3.3) are calculated in the proofs of Lemmas 3.10 (high frequencies) and 3.11 (low frequencies). For the nonoverlapping case, the proof of Theorem 4.1 gives the estimate of the convergence factor.

Proof of Lemma 3.9. We split this proof into three steps: the "high frequency" case (which is easier), leading to (3.8), and the "low frequency" case and the estimate of $\rho(T)$, which is harder and leads to (3.17).

Step 1. Consider first the frequencies $k \geq \pi/H$ which are unaffected by the coarse grid correction. For these frequencies, we will use (2.2) and (3.1) together to obtain an explicit recurrence for the Fourier coefficients $\hat{v}_j^n(x, k)$. This explicit recurrence is linear and the spectral radius of this recurrence can be analyzed with the help of (3.6).

On the subdomain Ω_0, the Robin transmission condition at $x = (H + L)/2$ is

$$(p + D_x)\hat{v}_0^{n+1}(x, k)|_{x=\frac{H+L}{2}} = (p + D_x)\hat{v}_1^n(x, k)|_{x=\frac{H+L}{2}}.$$

Substituting formula (3.1) leads to the equation

$$(p + k)e^{\frac{k(H+L)}{2}}\alpha_0^{n+1} + (p - k)e^{-\frac{k(H+L)}{2}}\beta_0^{n+1} = (p + k)e^{\frac{k(-H+L)}{2}}\alpha_1^n + (p - k)e^{-\frac{k(-H+L)}{2}}\beta_1^n.$$

Similarly, an equation for the Robin condition at $x = -(H + L)/2$ is obtained:

$$(p - k)e^{-\frac{k(H+L)}{2}}\alpha_0^{n+1} + (p + k)e^{\frac{k(H+L)}{2}}\beta_0^{n+1} = (p - k)e^{-\frac{k(-H+L)}{2}}\alpha_{-1}^n + (p + k)e^{\frac{k(-H+L)}{2}}\beta_{-1}^n.$$

Explicitly solving for $(\alpha_0^{n+1}, \beta_0^{n+1})^T$, produces the linear relation

$$\begin{bmatrix} \alpha_0^{n+1} \\ \beta_0^{n+1} \end{bmatrix} = \begin{bmatrix} a_{-1} & b_{-1} & 0 & 0 & a_1 & b_1 \\ b_1 & a_1 & 0 & 0 & b_{-1} & a_{-1} \end{bmatrix} \begin{bmatrix} \alpha_{-1}^n \\ \beta_{-1}^n \\ \alpha_0^n \\ \beta_0^n \\ \alpha_1^n \\ \beta_1^n \end{bmatrix},$$

where

$$a_{\pm 1} = \pm \frac{1}{d_0} e^{\pm kL} (k \pm p)^2,$$

$$b_{\pm 1} = \mp \frac{1}{d_0} e^{\pm kH} (k^2 - p^2), \quad \text{and}$$

$$d_0 = e^{k(H+L)} (k+p)^2 - e^{-k(H+L)} (k-p)^2.$$

It clearly follows that (3.8) holds. Let $\boldsymbol{\alpha}^n = [\alpha_1^n, \ldots, \alpha_J^n]^T$ and $\boldsymbol{\beta}^n = [\beta_1^n, \ldots, \beta_J^n]^T$, and the iteration can be rewritten in the form

$$\begin{bmatrix} \boldsymbol{\alpha}^{n+1} \\ \boldsymbol{\beta}^{n+1} \end{bmatrix} = T_k \begin{bmatrix} \boldsymbol{\alpha}^n \\ \boldsymbol{\beta}^n \end{bmatrix}, \tag{10.1}$$

with $T_k = T$ as in Lemma 3.7 and $a_0 = b_0 = 0$. The eigenvalues $\lambda_{j,\pm}$ are hence given by (3.6), and the upper bound (3.10) is given by (3.9).

Step 2. The technique is more or less the same as the one used for the high frequencies, but with the added complication of the coarse grid correction. Because the eigenvalues of T are more complicated in the low frequencies, we have an additional, final step to find a bound for the spectral radius $\rho(T)$.

For the frequencies $k < \pi/H$ and with $x \in [0, H]$, the coarse grid correction is the linear polynomial

$$\hat{z}^n(x, k) = \frac{H - x}{H} (\alpha_0^n + \beta_0^n) + \frac{x}{H} (\alpha_1^n + \beta_1^n).$$

A similar formula also holds in other x intervals. The algorithm with a coarse grid correction (CO0) has the following Robin transmission condition at $x = \frac{H+L}{2}$:

$$(p + D_x)\hat{v}_0^{n+1}(x, k)|_{x = \frac{H+L}{2}} = (p + D_x)(\hat{v}^n(x, k) - \hat{z}^n(x, k))|_{x = \frac{H+L}{2}}.$$

Using (3.1), the left-hand side is

$$(p + D_x)\hat{v}_0^{n+1}(x, k)|_{x = \frac{H+L}{2}} = e^{\frac{1}{2} k (H+L)} (p + k) \alpha_0^{n+1} + e^{-\frac{1}{2} k (H+L)} (p - k) \beta_0^{n+1}.$$

Similarly, the right-hand side is

$$(p + D_x)(\hat{v}^n(x, k) - \hat{z}^n(x, k))|_{x = \frac{H+L}{2}} = \frac{2 + (-H + L) p}{2H} \alpha_0^n + \frac{2 + (-H + L) p}{2H} \beta_0^n$$
$$+ \frac{2 H (p + k) e^{1/2 k (-H+L)} - 2 - pH - pL}{2H} \alpha_1^n + \frac{-2 H (-p + k) e^{-1/2 k (-H+L)} - 2 - pH - pL}{2H} \beta_1^n.$$

Similar relations can be obtained for the boundary condition at $x = -\frac{H+L}{2}$. The resulting recurrence can be written as

$$\begin{bmatrix} \alpha_0^{n+1} \\ \beta_0^{n+1} \end{bmatrix} = \begin{bmatrix} b_{-1} & a_{-1} & b_0 & a_0 & b_1 & a_1 \\ a_1 & b_1 & a_0 & b_0 & a_{-1} & b_{-1} \end{bmatrix} \begin{bmatrix} \beta_{-1}^n \\ \alpha_{-1}^n \\ \beta_0^n \\ \alpha_0^n \\ \beta_1^n \\ \alpha_1^n \end{bmatrix}, \tag{10.2}$$

which leads to an expression of the form (10.1), with $T_k = T$ as in Lemma 3.7, but now the entries of the matrix are given by (3.11)–(3.14), (3.15) and (3.16). Therefore, the eigenvalues are given by (3.6).

Step 3. We must now find an upper bound for $\rho(T_k)$ for the low frequencies which is sharp enough for our convergence analysis. This upper bound is essentially given by maximizing the eigenvalues (3.6) over the parameter j, which plays the role of a "coarse frequency".

The eigenvalues (3.6) are all of the form

$$\lambda_{k,z,\pm} = a_0 + (a_1 + a_{-1})z \pm \sqrt{\delta(z)}, \tag{10.3}$$

22

where the discriminant $\delta(z)$ is

$$\delta(z) = (b_0 + (b_1 + b_{-1}z))^2 + (b_1 - b_{-1})^2(1 - z^2) - (a_1 - a_{-1})^2(1 - z^2)$$
$$= (a_1 + a_{-1})^2 z^2 + 2b_0(b_1 + b_{-1})z + b_0^2 + b_1^2 + b_{-1}^2 - a_1^2 - a_{-1}^2 \qquad \text{(since } b_1 b_{-1} = a_1 a_{-1}),$$

and the variable $z = \cos 2\pi j/J$ ranges in the closed interval $[-1, 1]$. We proceed by finding six candidates for extrema, such that the maximum absolute value of these six candidates for extrema is an upper bound for $\rho(T_k)$. Notice that $\delta(\pm 1)$ is positive and that

$$\lambda_{k,1,\pm} = (a_0 + a_1 + a_{-1}) \pm (b_0 + b_1 + b_{-1}) \text{ and} \qquad (10.4)$$
$$\lambda_{k,-1,\pm} = (a_0 - a_1 - a_{-1}) \pm (b_0 - b_1 - b_{-1}). \qquad (10.5)$$

These form the first four candidates for extrema. Next, note that there is no interior extremum since $\partial\lambda_{k,z,\pm}/\partial z$ is nonzero (as long as $\delta > 0$). Observe that δ is a convex quadratic polynomial, and thus it is either non-negative over the entire range $[-1, 1]$, or possibly it is nonpositive over an interval $[z_1, z_2] \subset (-1, 1)$. If such an interval exists, it is possible that $\lambda_{k,z_j,\pm}$ is an extremum, $j = 1, 2$. In this situation, we derive a conservative upper bound as follows.

For values of z in the interval $[z_1, z_2]$, we have that

$$|\lambda_{k,z,\pm}|^2 = (a_0 + (a_1 + a_{-1})z)^2 + |\sqrt{\delta}|^2$$
$$= (a_0 + (a_1 + a_{-1})z)^2 - \delta \quad \text{(since } \delta \leq 0, \text{ hence } |\sqrt{\delta}|^2 = -\delta)$$
$$= p_k(z), \qquad (10.6)$$

where $p_k(z)$ is given by (3.20). If the number $p_k(z)$ is negative, then clearly the interval $[z_1, z_2]$ is empty. Then $\sqrt{p_k(z)}$ is not a candidate for an extremum, which is the effect of writing $\Re\sqrt{p_k(z)}$ in (3.17). On the other hand, if $p_k(z)$ is positive, then it will be used to produce two more candidates for extrema.

Since $p_k(z)$ is a linear polynomial, its maximum over the interval $z \in [z_1, z_2]$ is attained either at $z = z_1$ or $z = z_2$. Since no explicit formula for z_1 and z_2 is available, we use instead that $p_k(z) < \max(p_k(1), p_k(-1))$. This leads us to the final two candidates for extrema, $\sqrt{p_k(\pm 1)}$. $\quad\square$

Proof of Lemma 3.10. The challenge of this proof is to estimate $\sup_{k \geq \pi/H} |\rho_{p,L,H,+}(k)|$. Unfortunately, we were unable to find a "soft" way of doing this and instead the entire proof is based on difficult, tedious "hard" estimates.[10]

The convergence factor for $k \geq \pi/H$ is governed by $\rho_{p,L,H,\pm}$ as defined in (3.10). We thus consider several cases.

Case 1. First, consider $\rho_{p,L,H,+}$ given in (3.10). It turns out that the analysis is easier if we apply a change of variable to the k variable. To that end, we introduce the new variable s and we let $k = sp = sc\epsilon^{2/3}L^{-1}$. Thus,

$$\sup_{k \geq \pi/H} |\rho_{p,L,H,+}(k)| = \sup_{s \geq \pi c^{-1}\epsilon^{1/3}} |\rho_{c\epsilon^{2/3}L^{-1},L,L\epsilon^{-1},+}(s\pi c\epsilon^{2/3}L^{-1})|$$

$$= \sup_{s \geq \pi c^{-1}\epsilon^{1/3}} \frac{\left(e^{sc\epsilon^{2/3}} - e^{\frac{sc}{\epsilon^{1/3}}}\right)s + e^{sc\epsilon^{2/3}} + e^{\frac{sc}{\epsilon^{1/3}}}}{\left(-1 + e^{\frac{sc}{\epsilon^{1/3}}}e^{sc\epsilon^{2/3}}\right)s + 1 + e^{\frac{sc}{\epsilon^{1/3}}}e^{sc\epsilon^{2/3}}}. \qquad (10.7)$$

For frequencies $k \geq \pi/H$, the last expression is independent of the overlap L, and therefore so is the convergence factor. To compute this supremum, we consider the cases $\pi c^{-1}\epsilon^{1/3} \leq s \leq 1$ and $s \geq 1$ separately. Let $\rho_+(s) = \rho_{c\epsilon^{2/3}L^{-1},L,L\epsilon^{-1},+}(sc\epsilon^{2/3}L^{-1})$, as in (10.7). We make the substitutions $q = e^{sc\epsilon^{-1/3}} > 1$ and $r = e^{sc\epsilon^{2/3}} > 1$, and write

$$\rho_+(s) = \frac{(-s+1)q + rs + r}{(rs+r)q - s + 1} > 0.$$

---

[10]We would add that the authors had great difficulty finding this proof. The motivation for the substitution $k = sp$ (and splitting the s interval into many subintervals) has unfortunately been lost.

Case 1.a. For the range $\pi c^{-1}\epsilon^{1/3} \leq s \leq 1$, observe that $\rho_+(s)$ is a monotonically decreasing function of s. Indeed, the derivative of $\rho_+(s)$ with respect to s is

$$\frac{\overbrace{cr\,(q-1)\,(q+1)\,(s-1)\,(s+1)}^{<0}\,\epsilon - \overbrace{2\,r\,(q-1)\,(q+1)}^{>0}\,\epsilon^{1/3} - cq\overbrace{(-s+rs+1+r)}^{>0}\overbrace{(rs+r+s-1)}^{>0}}{\underbrace{(-s+sqr+1+qr)^2}_{>0}\,\epsilon^{1/3}} < 0.$$

Therefore, on the interval $s \in [\pi c^{-1}\epsilon^{1/3}, 1]$, the function $\rho_+(s)$ is maximized at $s = \pi c^{-1}\epsilon^{1/3}$.

Case 1.b. For $s > 1$, we can approximate ρ uniformly in s up to $O(e^{-c\epsilon^{-1/3}})$. We have

$$\rho_+(s) - \frac{1-s}{1+s}e^{-cs\epsilon^{2/3}} = \frac{(s+1)^2\,r^2 - (s-1)^2}{(rs+r)\,(s+1)\,rq + (-s+1)\,(s+1)\,r} \geq 0,$$

where we have used that $r > 1$ and $s > 0$. Hence,

$$0 \leq \rho_+(s) - \frac{1-s}{1+s}e^{-cs\epsilon^{2/3}} \leq \frac{(s+1)^2\,r^2 - (s-1)^2}{(rs+r)\,(s+1)\,rq} = O(e^{-c\epsilon^{-1/3}}),$$

as claimed. The function $\rho_\approx(s) := \frac{1-s}{1+s}e^{-cs\epsilon^{2/3}}$ has a unique extremum (a minimum) in $s > 1$, at $s_0 = \sqrt{2c^{-1}\epsilon^{-2/3}+1}$. Therefore, since $\rho_\approx$ attains its maximum at $s = 1$,

$$\rho_\approx(s_0) < \rho_+(s) < \rho_\approx(1) + O(e^{-c\epsilon^{-1/3}});$$

and since $\rho_\approx(1) = 0$,

$$\frac{1-s_0}{1+s_0}e^{-cs_0\epsilon^{2/3}} < \rho_+(s) < O(e^{-c\epsilon^{-1/3}}),$$

for all $s > 1$.

Thus, to conclude Case 1, when ϵ is sufficiently small, we have that

$$\rho_+(\pi c^{-1}\epsilon^{1/3}) \geq \rho_+(s) \geq \frac{1-s_0}{1+s_0}e^{-cs_0\epsilon^{2/3}},$$

for all $s \geq \pi c^{-1}\epsilon^{1/3}$. The bounds are independent of s, and thus taking a series expansion in ϵ of the upper and lower bounds, one obtains

$$1 - 2\frac{\pi\,(-1+e^\pi)}{c\,(e^\pi+1)}\epsilon^{1/3} + O\left(\epsilon^{2/3}\right) \geq \rho_+(s) \geq -1 + 2\sqrt{2c}\,\epsilon^{1/3} + O\left(\epsilon^{2/3}\right). \tag{10.8}$$

Case 2. A similar reasoning applies to $|\rho_{p,L,H,-}(k)|$. Define $\rho_-(s)$ from (3.10) by

$$\rho_-(s) = \rho_{c\epsilon^{2/3}L^{-1},L,L\epsilon^{-1},+}(sc\epsilon^{2/3}L^{-1})$$

$$= \frac{e^{sc\epsilon^{2/3}} + se^{sc\epsilon^{2/3}} + se^{\frac{sc}{\epsilon^{1/3}}} - e^{\frac{sc}{\epsilon^{1/3}}}}{e^{sc\epsilon^{2/3}}e^{\frac{sc}{\epsilon^{1/3}}} + se^{sc\epsilon^{2/3}}e^{\frac{sc}{\epsilon^{1/3}}} + s - 1}.$$

Case 2.a. On the range $s \in [\pi c^{-1}\epsilon^{2/3}, 1]$, ρ_- is monotonically increasing, when ϵ is small enough. We have

$$\rho_-'(s) = \frac{\overbrace{-r\left(ces^2 - ce - 2\,\epsilon^{1/3}\right)q^2 - c\,(sr+s+r-1)\,(sr-s+r+1)\,q + r\left(ces^2 - ce - 2\,\epsilon^{1/3}\right)}^{p(q)}}{(rq+srq+s-1)^2\,\epsilon^{1/3}}.$$

We have labeled the numerator $p(q)$. We now fix values of $s, \epsilon \in (0,1)$, also fixing $r = e^{sc\epsilon^{2/3}}$, but keeping q as a variable. Hence, we want to show that $p(e^{sc\epsilon^{-1/3}}) > 0$. To do this, we look at $p(q)$ as a quadratic polynomial

24

in the variable q. We will show that $p(q)$ is convex, and that if ϵ is small enough, then $p'(1 + sc\epsilon^{-1/3})$ is positive, implying that $p(q)$ is monotonically increasing for $q > 1 + sc\epsilon^{-1/3}$. Finally, we will show that $p(1 + sc\epsilon^{-1/3} + (sc\epsilon^{-1/3})^2/2) > 0$ if ϵ is sufficiently small. Since $q = e^{sc\epsilon^{-1/3}} > 1 + sc\epsilon^{-1/3} + (sc\epsilon^{-1/3})^2/2$, we will thus have shown that $p(e^{sc\epsilon^{-1/3}}) > 0$, if ϵ is sufficiently small.

First, observe that

$$p''(q) = 2\,rc\,(1-s)\,(s+1)\,\epsilon + 4\,r\epsilon^{1/3} > 0,$$

implying that $p(q)$ is a convex quadratic polynomial in q. Furthermore,

$$p'(1 + sc\epsilon^{-1/3}) = \overbrace{2\,rc\,(1-s)\,(s+1)\,\epsilon}^{>0} + \overbrace{2\,rc^2\,(1-s)\,(s+1)\,s\epsilon^{2/3}}^{>0} + \overbrace{4\,r\epsilon^{1/3}}^{>4\epsilon^{1/3}}$$
$$- c\,\underbrace{(r-1)}_{O(\epsilon^{2/3})}\,\underbrace{\left(s^2 r + 2\,sr + r - 2\,s + s^2 + 1\right)}_{O(1)} > 0,$$

so long as ϵ is sufficiently small. Finally, consider

$$p(1 + sc\epsilon^{-1/3} + (sc\epsilon^{-1/3})^2/2) = \overbrace{2\,rc^2\,(1-s)\,(s+1)\,s\epsilon^{2/3}}^{>0} + \overbrace{2\,rc^3\,(1-s)\,(s+1)\,s^2\epsilon^{1/3}}^{>0} + \overbrace{c^4 rs^3\left(1-s^2\right)}^{>0}$$
$$- \underbrace{\left(c + \frac{c^2 s}{\epsilon^{1/3}}\right)(r-1)\left((s+1)^2 r + (s-1)^2\right)}_{L} + \overbrace{1/4\frac{c^5 s^4 r\left(1-s^2\right)}{\epsilon^{1/3}}}^{>0}$$
$$- \underbrace{1/2\,\frac{c^3 s^2\,(r-1)\left(rs^2 + 2\,rs + r - 2\,s + s^2 + 1\right)}{\epsilon^{2/3}}}_{M} + \overbrace{1/2\frac{rs^4 c^4}{\epsilon}}^{N}.$$

Note the definitions of L, M, and N, in the last equation. We now analyze the quantity $N - L - M$ and show that it is positive, when ϵ is small, for all $s \in (c^{-1}\pi\epsilon^{1/3}, 1)$. Consider two cases, depending on whether $s \le \epsilon^{1/5}$ or $s \ge \epsilon^{1/5}$. In the first case, if $s \le \epsilon^{1/5}$, then we can estimate the values of L and M as follows

$$L = \overbrace{\left(c + \frac{c^2 s}{\epsilon^{1/3}}\right)}^{<c + c^2\epsilon^{-2/15}}\,\overbrace{(r-1)}^{O(\epsilon^{2/3})}\,\overbrace{\left((s+1)^2 r + (s-1)^2\right)}^{O(1)} = O(\epsilon^{8/15}),$$

$$M = 1/2\,\frac{\overbrace{c^3}^{}\,\overbrace{s^2}^{O(\epsilon^{2/5})}\,\overbrace{(r-1)}^{O(\epsilon^{2/3})}\,\overbrace{\left(rs^2 + 2\,rs + r - 2\,s + s^2 + 1\right)}^{O(1)}}{\epsilon^{2/3}} = O(\epsilon^{2/5}).$$

As for N, using the fact that $s \ge \pi c^{-1}\epsilon^{1/3}$, the following holds

$$N = 1/2\frac{rs^4 c^4}{\epsilon} \ge 1/2\pi^4\epsilon^{1/3}.$$

Therefore, when ϵ is sufficiently small, $N - L - M > 0$ for all $s \in [\pi c^{-1}\epsilon^{1/3}, \epsilon^{1/5}]$.

In the second case, if $s > \epsilon^{1/5}$, then we obtain

$$L = \overbrace{\left(c + \frac{c^2 s}{\epsilon^{1/3}}\right)}^{O(\epsilon^{-1/3})}\,\overbrace{(r-1)}^{O(\epsilon^{2/3})}\,\overbrace{\left((s+1)^2 r + (s-1)^2\right)}^{O(1)} = O(\epsilon^{1/3}),$$

$$M = 1/2\,\frac{c^3 s^2\,\overbrace{(r-1)}^{O(\epsilon^{2/3})}\,\overbrace{\left(rs^2 + 2\,rs + r - 2\,s + s^2 + 1\right)}^{O(1)}}{\epsilon^{2/3}} = O(1), \text{ and}$$

$$N = 1/2\frac{rs^4 c^4}{\epsilon} \ge 1/2rc^4\epsilon^{-1/5} = \Omega(\epsilon^{-1/5}).$$

(Recall that $\Omega(g)$ is a function bounded below by a constant times g, to be distinguished from the notation for the domain Ω.) Hence, for any sufficiently small ϵ, $N - L - M > 0$ for all $s \in [\epsilon^{1/5}, 1]$. Therefore,

$$p(e^{sc\epsilon^{-1/3}}) > p(1 + sc\epsilon^{-1/3} + (sc\epsilon^{-1/3})^2/2) > 0,$$

as required.

Consequently, $\rho'_-(s) > 0$ for all $s \in [\pi c^{-1}\epsilon^{1/3}, 1]$, as long as ϵ is sufficiently small, and the only candidates for extrema of ρ_- in the interval $\epsilon^{1/3}\pi c^{-1} \le s \le 1$ are on the boundary, at $s = \epsilon^{1/3}\pi c^{-1}$ and $s = 1$ (as long as ϵ is sufficiently small).

Case 2.b. For $s > 1$, we again use a uniform approximation as follows,

$$\rho_-(s) - \frac{s-1}{s+1}e^{-sc\epsilon^{2/3}} = \frac{(s+1)^2\,r^2 - (s-1)^2}{(s+1)^2\,r^2 q + r\,(s^2-1)} \ge 0,$$

which also leads to the following estimate

$$0 \le \rho_-(s) - \frac{s-1}{s+1}e^{-sc\epsilon^{2/3}} \le \overbrace{\left(\frac{(s+1)^2 r^2 - (s-1)^2}{(s+1)^2 r^2}\right)}^{O(1)}\frac{1}{q} = O(1/q) = O(e^{-c\epsilon^{-1/3}}).$$

This time, the uniform approximation does not yield a conservative bound, but it does yield a uniformly good estimate. Concluding Case 2, for every $s > \pi c^{-1}\epsilon^{1/3}$,

$$\rho_-(s) \in Hull\left\{\rho_-(\pi c^{-1}\epsilon^{1/3}), \rho_-(1), \frac{s_0-1}{s_0+1}e^{-s_0 c\epsilon^{2/3}} + O(e^{-c\epsilon^{-1/3}})\right\},$$

where $Hull(E)$ is the closed interval $[\inf E, \sup E]$. Taking a series expansion in ϵ, we obtain

$$-1 + 2\frac{\pi\,(1+e^\pi)}{c\,(e^\pi - 1)}\epsilon^{1/3} + O\left(\epsilon^{2/3}\right) \le \rho_-(s) \le 1 - 2\sqrt{2c}\,\epsilon^{1/3} + O\left(\epsilon^{2/3}\right). \tag{10.9}$$

Putting (10.8) and (10.9) together, the desired estimate (3.21) is obtained. □

Proof of Lemma 3.11. Let $\boldsymbol{\alpha}^n = [\alpha_1^n, \ldots, \alpha_J^n]^T$ and $\boldsymbol{\beta}^n = [\beta_1^n, \ldots, \beta_J^n]^T$ be the vectors containing the Fourier coefficients of the iterates as in (3.1). Following Lemma 3.9, the iteration becomes

$$\begin{bmatrix} \boldsymbol{\alpha}^{n+1} \\ \boldsymbol{\beta}^{n+1} \end{bmatrix} = \begin{bmatrix} A & B \\ B^* & A^* \end{bmatrix}\begin{bmatrix} \boldsymbol{\alpha}^n \\ \boldsymbol{\beta}^n \end{bmatrix},$$

where A, B are as in Lemma 3.7. The eigenvalues $\lambda_{j,\pm}$ are given by (3.6), and we may use the upper bound $\rho_{p,L,H}$ defined in (3.17) for the convergence factor. Therefore, we will analyze the candidates for extrema (3.18), (3.19) and (3.20), by substituting $p = c\epsilon^{2/3}L^{-1}$, $H = \epsilon^{-1}L$ and $k = \epsilon s/L$.

For the first candidate extremum, we obtain

$$\lambda_{1,+}(s) := \lambda_{\epsilon s L^{-1},1,+}$$
$$= \frac{\epsilon^{2/3}\,(r+q)\,(r-q)\,(q^2 v^2 + 1)\,s^2 + 2\,\epsilon^{1/3}cq\,(r^3 q - 1)\,(r-q)\,s + c^2\,(rq-1)\,(rq+1)\,(r-q)^2}{\epsilon^{2/3}\,(rq-1)\,(rq+1)\,(q^2 r^2 + 1)\,s^2 + 2\,\epsilon^{1/3}c\,(q^4 r^4 + 1)\,s + c^2\,(rq-1)\,(rq+1)\,(q^2 r^2 + 1)},$$

where we have used the shorthand $q = e^{s/2}$ and $r = e^{\epsilon s/2}$. Note that s ranges in the interval $[0, \pi]$, and thus $1 \le q \le e^{\pi/2} \approx 4.82$ and $1 \le r \le q$, when $0 < \epsilon < 1$. We next show that, if ϵ is sufficiently small, then $\lambda_{1,+}(s) \ge 0$ for all $s \in [0, \pi]$. We first show that $\lambda_{1,+}(s) \ne 0$. To that end, assume that q and r are fixed (and not functions of s) and solve $\lambda_{1,+}(s) = 0$ for the unknown s, obtaining

$$s = \frac{c\,(q-r)}{\epsilon^{1/3}\,(r+q)}.$$

One easily verifies that $q - r \ge \frac{1-\epsilon}{2}s$ and $(r+q) \le 2q < 10$, hence

$$s \ge c\frac{1-\epsilon}{20\epsilon^{1/3}}s.$$

26

Dividing across by s (if it is nonzero), a contradiction is reached, when ϵ is small. Thus, $\lambda_{1,+}(s)$ does not have a zero in the interval $(0, \pi]$. Furthermore, we have that

$$\lambda_{1,+}(1) = \frac{\overbrace{-\left(e^{\epsilon/2} + e^{1/2}\right)\left(-e^{\epsilon/2} + e^{1/2}\right)\epsilon^{1/3}}^{O(\epsilon^{1/3})} + \overbrace{\left(-e^{\epsilon/2} + e^{1/2}\right)^2 c}^{\Omega(1)}}{\left(e^{1+\epsilon} - 1\right)\epsilon^{1/3} + c\left(e^{1+\epsilon} + 1\right)} > 0,$$

if ϵ is sufficiently small.

Next, we find an upper bound for $\lambda_{1,+}(s)$. To that end, define

$$\ell(\epsilon) := \frac{(q-1)^2}{1+q^2} - \lambda_{1,+}(s)$$

$$= \frac{\left(\epsilon^{1/3}s + r^2c - c + sr^2\epsilon^{1/3}\right)q^4 - 2\,r\left(rc + r\epsilon^{1/3}s - c\right)q^3 + \left(2\,rc + 2\,\epsilon^{1/3}s - 2\,c\right)q + c - \epsilon^{1/3}s - sr^2\epsilon^{1/3} - r^2c}{r^2\left(\epsilon^{1/3}s + c\right)q^4 + \left(-\epsilon^{1/3}s + c + sr^2\epsilon^{1/3} + r^2c\right)q^2 - \epsilon^{1/3}s + c},$$

and the aim is to show that $\ell(\epsilon) > 0$ for all $s \in [0, 1]$ thus obtaining an upper bound. In order to do this, assume that q and r are fixed (and not functions of ϵ), and solve $\ell(\epsilon) = 0$ for the unknown ϵ, obtaining

$$\epsilon = -\frac{c^3\,(r-1)^3\left(rq^4 - 2\,rq^3 - r + 2\,q - 1 + q^4\right)^3}{s^3\left(q^4r^2 - 2\,q^3r^2 - r^2 + q^4 + 2\,q - 1\right)^3}. \tag{10.10}$$

We now compute the sign of the right hand side of (10.10). Consider the expression

$$p(q) = rq^4 - 2\,rq^3 - r + 2\,q - 1 + q^4$$

as a polynomial in q. Observe that $p''(q) = 12\,(r+1)\,q^2 - 12\,rq > 0$, since $q > 1$ (and thus $q^2 > q$), and $r > 1$. Therefore, p is convex. Furthermore, $p'(1) = 6 - 2r \geq 6 - 2e^{\epsilon\pi/2} > 0$, if ϵ is sufficiently small. Consequently, $p(q)$ is monotonically increasing for $q \geq 1$. Finally, $p(r) = r^5 - r^4 + r - 1 > 0$ whenever $r > 1$, and $p(q) > 0$ whenever $q > r$. A similar reasoning applies to the denominator, showing that it is positive. Hence, we have that $\epsilon < 0$, which contradicts $\epsilon > 0$, implying that $\ell(\epsilon)$ is nonzero. Finally, by substituting values of ϵ, c, s we find that $\ell(\epsilon) > 0$. Furthermore,

$$0 \leq \lambda_{1,+}(s) \leq \frac{(q-1)^2}{1+q^2} < 0.61 \quad (\text{since } 1 \leq q < 4.82),$$

for every $0 \leq s \leq \pi$, as long as ϵ is sufficiently small. As a consequence, $|\lambda_{1,+}|$ can be removed from consideration, since it will not be an upper bound for the convergence factor ρ.

The second candidate extremum is

$$\lambda_{1,-}(s) := \lambda_{\epsilon s L^{-1}, 1, -}$$

$$= \frac{\overbrace{s\,(qr+1)\,(qr-1)\left(r^2+q^2\right)\epsilon^{2/3}}^{O(\epsilon^{2/3})} + \overbrace{2\,q^2c\left(r^4+1\right)\epsilon^{1/3}}^{O(\epsilon^{1/3})} + \overbrace{c^2\,(r-q)\,(r+q)\left(q^2r^2+1\right)s^{-1}}^{\Omega(1)}}{\underbrace{s\,(qr-1)\,(qr+1)\left(q^2r^2+1\right)\epsilon^{2/3}}_{O(\epsilon^{2/3})} + \underbrace{2\,c\left(r^4q^4+1\right)\epsilon^{1/3}}_{O(\epsilon^{1/3})} + \underbrace{c^2\,(qr-1)\,(qr+1)\left(q^2r^2+1\right)s^{-1}}_{\Omega(1)}}$$

where the $O(\epsilon^{(\cdot)})$ are positive and tend to zero uniformly at the appropriate rate, and the terms $\Omega(1)$ have a magnitude greater than some constant. To see that this constant is independent of s, note that $q - r \geq \frac{1-\epsilon}{2}s$, or equivalently, $s^{-1}(q-r) \geq \frac{1-\epsilon}{2}$. Similarly, $s^{-1}(qr-1) \geq \frac{1+\epsilon}{2}$, and since $r < q$, when ϵ is sufficiently small, $\lambda_{1,-}(s)$ is negative for every $s \in (0, \pi]$. We can further obtain a lower bound for $\lambda_{1,-}(s)$ by neglecting the $O(\epsilon^{(\cdot)})$ terms on the denominator (since they are positive), and by neglecting the $O(\epsilon^{2/3})$ on the numerator (since it is also positive), obtaining

$$\lambda_{1,-} \geq 2\,\frac{\epsilon^{1/3}q^2\left(r^4+1\right)s}{c\,(qr-1)\,(qr+1)\left(q^2r^2+1\right)} + \frac{(r-q)\,(r+q)}{(qr-1)\,(qr+1)}$$

$$\geq \frac{-c + c\epsilon + 2\,\epsilon^{1/3}}{c + c\epsilon} = -1 + \frac{2}{c}\epsilon^{1/3} + O(\epsilon).$$

27

We analyze $\lambda_{k,-1,+}$ and $\lambda_{k,-1,-}$ in a similar way, obtaining

$$0 \geq \lambda_{k,-1,+} \geq \frac{4\,\epsilon^{4/3} + 4\,\epsilon^2 c - c^2 \epsilon^{2/3} + c^2 \epsilon^{8/3}}{c\left(2\,\epsilon + \epsilon^{2/3}c + \epsilon^{5/3}c\right)} = -1 + \frac{2}{c}\epsilon^{1/3} + O(\epsilon) \text{ and}$$

$$0 \leq \lambda_{k,-1,-} \leq -\frac{2\,\epsilon - c\epsilon^{2/3} + c\epsilon^{5/3}}{2\,\epsilon + c\epsilon^{2/3} + c\epsilon^{5/3}} = 1 - \frac{4}{c}\epsilon^{1/3} + O(\epsilon^{2/3}),$$

if ϵ is sufficiently small.

Finally, if ϵ is sufficiently small, then $p_k(1)$ and $p_k(-1)$ (cf. (3.20)) are both negative, and do not need to be considered. Putting together the estimates for (3.18), (3.19), and (3.20), one obtains (3.22). □

Proof of Theorem 4.1. Like much of the proofs of the results in Section 3, the proof of this theorem is a highly technical piece of "hard analysis", although it is significantly easier than the other proofs in this Appendix. We divide our proof into two steps, first on the high frequencies, and then on the low frequencies.

Step 1. We begin by considering the high frequencies. For $k \geq \pi/H$, consider $\rho_{p,0,H,\pm}(k)$ given by (3.10), and by setting $q = e^{kH} > 1$, we have

$$\rho_{p,0,H,+}(k) = -\frac{k\,q - k - qp - p}{k\,q - k + qp + p} \quad \text{and} \quad \rho_{p,0,H,-}(k) = \frac{k\,q + k - qp + p}{k\,q + k + qp - p}.$$

Differentiating with respect to k, we obtain

$$\rho'_{p,0,H,+}(k) = -2\,\frac{p\left(q^2 + 2\,k\,Hq - 1\right)}{(k\,q - k + qp + p)^2} < 0,$$

since $q^2 - 1 > 0$. Similarly, one obtains

$$\rho'_{p,0,H,-}(k) = -2\,\frac{p\left(-e^{2\,k\,H} + 2\,k\,He^{k\,H} + 1\right)}{(k\,e^{k\,H} + k + e^{k\,H}p - p)^2} = -\frac{2p\sum_{j=1}^{\infty}\overbrace{\frac{j! - 2^{j-1}(j-1)!}{j!(j-1)!}}^{\leq 0}(kH)^j}{(ke^{kH} + k + e^{kH}p - p)^2} > 0.$$

Therefore, both $\rho_{p,0,H,-}(k)$ and $\rho_{p,0,H,+}(k)$ are monotonic over the interval $k \in [\pi/H, \pi/h]$ and thus

$$\sup_{k\in[\pi/H,\pi/h]} \rho_{p,0,H}(k) = \max\{|\rho_{p,0,H,+}(\pi/H)|, |\rho_{p,0,H,-}(\pi/H)|, |\rho_{p,0,H,+}(\pi/h)|, |\rho_{p,0,H,-}(\pi/h)|\}$$

$$= 1 - \frac{2c}{\pi}\epsilon^{1/2} + O(\epsilon). \tag{10.11}$$

Step 2. We now consider the low frequencies $k < \pi/H$. The six critical values $\lambda_{k,1,\pm}(p,0,H)$, $\lambda_{k,-1,\pm}(p,0,H)$, $p_k(\pm 1, p, 0, H)$ are given by equations (3.18), (3.19), and (3.20). The analysis is very similar to the procedure we followed in Lemma 3.11, but with many differences in the details, and we briefly outline the various comparisons and estimates we use.

For $\lambda_{1,+}$, let $q = e^{sc/2}$ and write

$$\lambda_{1,+} = \lambda_{sc\epsilon/h,1,+}(c\epsilon^{1/2}h^{-1}, 0, h/\epsilon) = (q-1)\frac{-\overbrace{(q+1)\,\epsilon^{1/2}}^{O(\epsilon^{1/2})} + \overbrace{(q-1)/s}^{>c/2}}{(q-1)\,(q+1)\,\epsilon^{1/2} + (q^2+1)\,/s}.$$

Note the slightly different substitutions than the ones used in Lemma 3.11; however, the argument used in the proof of Lemma 3.11 that shows that $\lambda_{1,+} \geq 0$ for sufficiently small ϵ is essentially the same. The range of the frequency parameter $k < \pi/H$ leads to $s < \pi/c$. We continue as in Lemma 3.11, comparing $\lambda_{1,+}$ and $(q-1)^2/(q^2+1)$. For all $0 < \epsilon < 1$, we find that $\lambda_{1,+} < (q-1)^2/(q^2+1)$. Hence, $0 < \lambda_{1,+} < 0.61$ and $\lambda_{1,+}$ plays no role in determining the convergence factor of the iteration.

28

The remaining critical values are

$$\lambda_{1,-} = \lambda_{sc\epsilon/h,1,-}(c\epsilon^{1/2}h^{-1},0,h/\epsilon) = \frac{\overbrace{(q^2+1)\sqrt{\epsilon}}^{O(\epsilon^{1/2})} - \overbrace{\left(\dfrac{q-1}{s}\right)(q+1)}^{\Omega(1)}}{(q^2+1)\sqrt{\epsilon} + \frac{(q-1)(q+1)}{s}},$$

$$\lambda_{-1,+} = \lambda_{sc\epsilon/h,-1,+}(c\epsilon^{1/2}h^{-1},0,h/\epsilon) = \frac{\overbrace{(-sc+4q+scq^2)\sqrt{\epsilon}}^{O(\epsilon^{1/2})} - \overbrace{c(q^2+1)}^{\Omega(1)}}{cs(q-1)(q+1)\sqrt{\epsilon} + c(q^2+1)},$$

$$\lambda_{-1,-} = \lambda_{sc\epsilon/h,-1,-}(c\epsilon^{1/2}h^{-1},0,h/\epsilon) = \frac{\overbrace{-(q^2+1)\sqrt{\epsilon}}^{O(\epsilon^{1/2})} + \overbrace{\left(\dfrac{q-1}{s}\right)(q+1)}^{\Omega(1)}}{(q^2+1)\sqrt{\epsilon} + \left(\frac{q-1}{s}\right)(q+1)},$$

$$p_{sc\epsilon/h}(1,c\epsilon^{1/2}/h,0,h/\epsilon) = \frac{\overbrace{-\dfrac{(q-1)(q+1)(q^2+1)\epsilon}{s}}^{O(\epsilon)} + 2\overbrace{\dfrac{(q-1)^2(q^2+q+1)\sqrt{\epsilon}}{s^2}}^{O(\epsilon^{1/2})} - \overbrace{\dfrac{(q-1)^3(q+1)}{s^3}}^{\Omega(1)}}{\frac{(q-1)(q+1)(q^2+1)\epsilon}{s} + 2\frac{(q^4+1)\sqrt{\epsilon}}{s^2} + \frac{(q-1)(q+1)(q^2+1)}{s^3}}, \text{ and}$$

$$p_{sc\epsilon/h}(-1,c\epsilon^{1/2}/h,0,h/\epsilon)$$

$$= \frac{\overbrace{-h(q^2+1)(-sc+4q+scq^2)\epsilon}^{O(\epsilon)} + 2\overbrace{\dfrac{h\left(c(1+q^4)s - 2q(q-1)(q+1)\right)\sqrt{\epsilon}}{s}}^{O(\epsilon^{1/2})} - \overbrace{\dfrac{hc(q-1)(q+1)(q^2+1)}{s}}^{\Omega(1)}}{hcs(q-1)(q+1)(q^2+1)\epsilon + 2hc(q^4+1)\sqrt{\epsilon} + \frac{hc(q-1)(q+1)(q^2+1)}{s}};$$

where we have used repeatedly that $(q-1)/s \geq c/2$ and $(q-1)/s = O(1)$. Furthermore, we obtain

$$\lambda'_{1,-} = -2\frac{\sqrt{\epsilon}\left(-e^{2\,sc} + 2\,sce^{sc} + 1\right)}{\left(\sqrt{\epsilon}se^{sc} + \sqrt{\epsilon}s + e^{sc} - 1\right)^2} > 0,$$

and hence

$$0 \geq \lambda_{1,-}(k) \geq \lambda_{1,-}(0) = \frac{-c + 2\sqrt{\epsilon}}{2\sqrt{\epsilon} + c} = -1 + \frac{4}{c}\epsilon^{1/2} + O(\epsilon).$$

For $\lambda_{-1,+}$, we have

$$\lambda'_{-1,-} = \frac{\left(\left(\overbrace{-2cq(q^2+1) - 4\dfrac{q(q-1)(q+1)}{s}}^{O(\epsilon^{1/2})}\right)\sqrt{\epsilon} + \overbrace{4c^2q^2 + 2\dfrac{c(q-1)(q+1)(q^2-q+1)}{s}}^{\Omega(1)}\right)s\sqrt{\epsilon}}{c\left(-\sqrt{\epsilon}s + \sqrt{\epsilon}sq^2 + q^2 + 1\right)^2} > 0,$$

and similarly for the other critical values, leading to the approximations

$$|\lambda_{-1,+}| \leq 1 - \frac{2}{c}\sqrt{\epsilon},$$

$$|\lambda_{-1,-}| \leq 1 - \frac{4}{c}\sqrt{\epsilon} + O(\epsilon).$$

Putting together (10.11) and the estimates for $|\lambda_{\pm 1,\pm}|$, one obtains (4.1).

To obtain the divergence result, note that

$$\lambda_{0,-1,+}(p,0,H) = \frac{2}{pH} - 1 \geq 1,$$

if $p < 1/H$. $\quad\square$

REFERENCES

[1] A. Alonso-Rodriguez and L. Gerardo-Giorda, New non-overlapping domain decomposition methods for the time-harmonic Maxwell system. *SIAM Journal on Scientific Computing*, 28:102–122, 2006.

[2] S. Balay, K. Buschelman, W. D. Gropp, D. Kaushik, M. G. Knepley, L. C. McInnes, B. F. Smith and H. Zhang, PETSc Web page, 2001. http://www.mcs.anl.gov/petsc

[3] D. Bennequin, M. J. Gander and L. Halpern, A homographic best approximation problem with application to optimized Schwarz waveform relaxation. *Mathematics of Computation*, 78:185–223, 2009.

[4] G. Bhanot, J. M. Dennis, J. Edwards, W. Grabowski, M. Gupta; K. Jordan, R. D. Loft, J. Sexton, A. St-Cyr, S. J. Thomas, H. M. Tufo, T. Voran, R. Walkup and A. A. Wyszogrodski, Early experiences with the 360TF IBM Blue gene/L platform. *International Journal of Computational Methods*, 5:237–253, 2008.

[5] X.-C. Cai and M. Sarkis, A restricted additive Schwarz preconditioner for general sparse linear systems. *SIAM Journal on Scientific Computing*, 21:792–797, 1999.

[6] P. Chevalier and F. Nataf, Symmetrized method with optimized second-order conditions for the Helmholtz equation. *Contemporary Mathematics*, 218:400–407, 1998.

[7] C. Chniti, F. Nataf and F. Nier, Improved interface conditions for a non-overlapping domain decomposition of a non-convex polygonal domain. *Comptes Rendus de l'Académie des Sciences*, 342:883–886, 2006.

[8] Q. Deng, An optimal parallel nonoverlapping domain decomposition iterative procedure. *SIAM Journal on Numerical Analysis*, 41:964–982, 2003.

[9] V. Dolean, M. J. Gander and L. Gerardo-Giorda, Optimized Schwarz methods for Maxwell's equations. *SIAM Journal on Scientific Computing*, 31:2193–2213, 2009.

[10] V. Dolean, S. Lanteri and F. Nataf, Optimized interface conditions for domain decomposition methods in fluid dynamics. *International Journal on Numerical Methods in Fluids*, 40:1539–1550, 2002.

[11] O. Dubois and M. J. Gander, Convergence behavior of a two-level optimized Schwarz preconditioner. In M. Bercovier, M. J. Gander, R. Kornhuber and O. Widlund (editors), Domain Decomposition Methods in Science and Engineering XVIII, Lecture Notes in Computational Science and Engineering, vol. 70, Springer, pp. 177–184, 2009.

[12] O. Dubois, Optimized Schwarz methods for the advection-diffusion equation and for problems with discontinuous coefficients. PhD thesis, Department of Mathematics and Statistics, McGill University, 2007.

[13] E. Efstathiou and M. J. Gander, Why restricted additive Schwarz converges faster than additive Schwarz. *BIT Numerical Mathematics*, 43:945-959, 2003.

[14] A. Frommer and D. B. Szyld. An algebraic convergence theory for restricted additive Schwarz methods using weighted max norms. *SIAM Journal on Numerical Analysis*, 39:463-479, 2001.

[15] M. J. Gander, Optimized Schwarz methods. *SIAM Journal on Numerical Analysis*, 44:699–731, 2006.

[16] M. J. Gander, Schwarz methods in the course of time, *Electronic Transactions on Numerical Analysis*, 31:228–255, 2008.

[17] M. J. Gander and L. Halpern, Absorbing boundary conditions for the wave equation and parallel computing. *Mathematics of Computations*, 74:153–176, 2004.

[18] M. J. Gander and L. Halpern, Optimized Schwarz waveform relaxation for advection reaction diffusion problems. *SIAM Journal on Numerical Analysis*, 45:666–697, 2007.

[19] M. J. Gander, L. Halpern and C. Japhet, Optimized Schwarz algorithms for coupling convection and convection-diffusion problems. In N. Debit, M. Garbey, R. Hoppe, J. Périaux, D. Keyes, Y. Kuznetsov, editors, *Proceedings of the Thirteenth International Conference on Domain Decomposition Methods*, pages 253-260. ddm.org, 2001.

[20] M. J. Gander, L. Halpern and F. Nataf, Optimal convergence for overlapping and non-overlapping Schwarz waveform relaxation. In C.-H. Lai, P. E. Bjorstad, M. Cross and O. Widlund, editors, *Proceedings of the Eleventh International Conference on Domain Decomposition Methods*, pages 27–36. ddm.org, 1999.

[21] M. J. Gander, L. Halpern and F. Nataf, Optimal Schwarz waveform relaxation for the one dimensional wave equation. *SIAM Journal on Numerical Analysis*, Vol. 41, No. 5, pp. 1643–1681, 2003.

[22] M. J. Gander, F. Magoules and F. Nataf, Optimized Schwarz methods without overlap for the Helmholtz equation. *SIAM Journal on Scientific Computing*, 24:38–60, 2002.

[23] C. Japhet, Conditions aux limites artificielles et décomposition de domaine: Méthode OO2 (Optimisé d'ordre 2). Application à la résolution de problèmes en mécanique des fluides. CMAP (Ecole Polytechnique), 1997, no. 373.

[24] C. Japhet, Optimized Krylov-Ventcell method. Application to convection-diffusion problems. In P. E. Bjørstad and M. S. Espedal and D. E. Keyes, editors, *Proceedings of the Ninth International Conference on Domain Decomposition Methods*, 1998, pages 382–389, ddm.org.

[25] C. Japhet, F. Nataf, F. Rogier, The Optimized Order 2 Method. Application to convection-diffusion problems. *Future Generation Computer Systems*, 18:17–30, 2001.

[26] J.-H. Kimn, A convergence theory for an overlapping Schwarz algorithm using discontinuous iterates. *Numerische Mathematik*, 100:117–139, 2005.

[27] P.-L. Lions, On the Schwarz alternating method III: a variant for non-overlapping subdomains. In T. F. Chan and R. Glowinski, J. Périaux and O. Widlund *Third international symposium on domain decomposition methods for partial differential equations*, SIAM, Philadelphia, pages 47–70, 1990.

[28] S. Loisel, J. Côté, M. J. Gander, L. Laayouni and A. Qaddouri, Optimized domain decomposition methods for the spherical Laplacian. SIAM Journal on Numerical Analysis, 44:524–551, 2010.

[29] S. Loisel and D. B. Szyld, On the convergence of Algebraic Optimizable Schwarz Methods with applications to elliptic problems. Numerische Mathematik, 114:697–728, 2009.

[30] S. H. Lui, A Lions non-overlapping domain decomposition method for domains with an arbitrary interface. IMA Journal of Numerical Analysis, 29:332–349, 2009.

[31] G. Lube, L. Mueller and F.-C. Otto, A non-overlapping domain decomposition method for the advection-diffusion problem. *Computing*, 64:49–68, 2000.

[32] Y. Maday and A. T. Patera, *Spectral element methods for the Navier-Stokes equations*. In state-of-the-art surveys on

computational mechanics. American Society of Mechanical Engineers, New York, 1989.

[33] V. Martin, An optimized Schwarz waveform relaxation method for unsteady convection diffusion equation. *Applied Numerical Mathematics*, 52:401–428, 2005.

[34] V. Martin, Schwarz waveform relaxation algorithms for the linear viscous equatorial shallow water qquations. *SIAM Journal on Scientific Computing*, 31:3595–3625, 2009.

[35] R. Nabben and D. B. Szyld, Convergence theory of restricted multiplicative Schwarz methods. *SIAM Journal on Numerical Analysis*, 40:2318–2336, 2003.

[36] F. Nataf, Absorbing boundary conditions in block Gauss-Seidel methods for convection problems. *Mathematical Models and Methods in Applied Sciences*, 6:481–502, 1996.

[37] F. Nataf and F. Nier, Convergence rate of some domain decomposition methods for overlapping and nonoverlapping subdomains. *Numerische Mathematik*, 75:357–77, 1997.

[38] A. T. Patera, A spectral element method for fluid dynamics: Laminar flow in a channel expansion. *Journal of Computational Physics*, 54:468–488, 1984.

[39] A. Qaddouri, L. Laayouni, S. Loisel, J. Côté and M. J. Gander, Optimized Schwarz methods with an overset grid for the shallow-water equations: preliminary results. *Applied Numerical Mathematics*, 58:459-471, 2008.

[40] A. Quarteroni and A. Valli, *Domain Decomposition Methods for Partial Differential Equations*. Oxford University Press, Oxford and New York, 1999.

[41] J. Reisner, A. Wyszogrodzki, V. Mousseau and D. Knoll, An efficient physics-based preconditioner for the fully implicit solution of small-scale thermally driven atmospheric flows. *Journal of Computational Physics*, 189:30–44, 2003.

[42] A. St-Cyr, M. J. Gander and S. J. Thomas, Optimized multiplicative, additive and restricted additive Schwarz preconditioning. *SIAM Journal on Scientific Computing*, 29:2402–2425, 2007.

[43] A. St-Cyr and S. J. Thomas, Nonlinear operator integration factor splitting for the shallow water equations. *Applied Numerical Mathematics*, 52:429–448, 2005.

[44] A. Stanifoth and J. Côté, Semi-Lagrangian integration schemes for atmospheric models – a review. *Monthly Weather Review* 119:2206–2222, 1991.

[45] A. Toselli and O. B. Widlund, *Domain Decomposition Methods - Algorithms and Theory*, volume 34 of *Springer Series in Computational Mathematics*. Springer, Berlin, Heidelberg, 2005.

[46] D. L. Williamson, J. B. Drake, J. J. Hack, R. Jakob and P. N. Swarztrauber, A standard test set for numerical approximations to the shallow water equations on the sphere. *Journal of Computational Physics*, 102:221–224, 1992.